DFT Study of Electronic, Optical and Thermoelectric Properties of Doped and Undoped Calcium Oxide

Aamir Khan
Reg No: 00000321382

A thesis submitted in partial fulfillment of the requirements
for the degree of **Master of Science**
in
Physics

Supervised by
Dr. Faheem Amin

Co-supervised by
Dr. Yasir Saeed

Department of Physics, School of Natural Sciences (SNS)
National University of Sciences and Technology (NUST)
Islamabad, Pakistan
2022

FORM TH-4

National University of Sciences & Technology

MS THESIS WORK

We hereby recommend that the dissertation prepared under our supervision by: Aamir Khan, Regn No. 00000321382 Titled: DFT Study of Electronic, Optical and Thermoelectric Properties of Doped and Un-Doped Calcium Oxide be Accepted in partial fulfillment of the requirements for the award of **MS** degree.

Examination Committee Members

1. Name: PROF. SYED RIZWAN HUSSAIN Signature: _____

2. Name: DR. FAHAD AZAD Signature: _____

Supervisor's Name DR. FAHEEM AMIN Signature: _____

Co-Supervisor's Name DR. YASIR SAEED Signature: _____

_____
Head of Department

06-07-2022
Date

COUNTERSINGED

Date: 06/07/2022

Dean/Principal

Acknowledgements

I would like to express my deepest gratitude to my supervisor Dr. Faheem Amin and co supervisor Dr. Yasir Saeed (AUST) for being very kind and helping throughout this project, as this could not have been possible, without their kind support. I would like to pay regards to my GEC members Professor Dr. Syed Rizwan Hussain and Dr. Fahad Azad for their valuable guidance. I am thankful to Dr. Fouzia Perveen (SINES), for her valuable support in this work. I am forever grateful to my parents for their unwavering support throughout my educational journey. Lastly, I am very thankful to all my friends for the helpful discussions and cheerful distractions.

Abstract

Calcium Oxide is a potential candidate for thermal energy storage at high temperatures in the range of 450-600 °C. the reversible solid gas reaction of $Ca(OH)_2/CaO$ system offers high energy density, long storage period and cost effectiveness. Our aim in this work is to explore it as a potential thermoelectric and optoelectronic material by tuning its band gap by different metal doping and creation of oxygen vacancies. Density functional theory technique is used to model the electronic, optical, and thermoelectric properties of modified and unmodified materials. Calcium oxide is a wide band gap material having an indirect band gap of 6.0 eV while a direct band gap of 7.1 eV has been determined experimentally. Therefore, to tune its band gap, it was doped with cadmium and zinc (25% each), while 25% and 3.12% oxygen vacancies were created in pure CaO. it was found that the indirect band gap was reduced to 4.47 eV and 4.25 eV for Zn and Cd doping respectively, while 25% and 3.12% oxygen vacancy reduced the band gap to 1.51 eV and 3.19 eV respectively. CaO with 3.12% Oxygen vacancy was found to have the highest figure of merit which makes it potential thermoelectric material. In the visible region, 25% Oxygen doped was found to have the highest absorption compared to all systems which makes it potential material for solar cell fabrication

Acronyms

Following are the list of abbreviations used throughout the thesis:

DFT	Density Functional Theory
CaO	Calcium Oxide
MgO	Magnesium Oxide
Zn	Zinc
Cd	Cadmium
AEO	Alkaline Earth Oxides
TE	Thermoelectric
PBE	Perdew Burke Ernzerhof
GGA	Generalized Gradient Approximation
LDA	Local Density Approximation
TB	Trans Blaha
mBJ	modified Backe Johnson
KS	Kohn Sham

Table of Contents

Acronyms

Topic **Page No.**

List of Figures

List of Tables

Chapter 1

Introduction

Energy consumption has risen in recent years as populations have grown and other resources like oil and gas (whose residuals are harmful) have been depleted. The cost-effective and environmentally friendly solutions to this energy crisis must be discovered. Green and renewable energy ways are piquing the researcher's interest to improve their efficiency and making them more practical. Our task in this thesis is to study the thermometric behavior of Calcium Oxide and study its optoelectronic properties for green and clean energy generation.

Thermoelectric devices require heat energy to produce electrical energy and optoelectronic devices require light as input to produce electrical energy. Solar radiation is the main source of heat and light energy. Because of its impact on living matter and the possibility of using them for constructive purposes, solar radiation is becoming increasingly valued. Because of its quantity and accessibility, it is a constant source of energy that, when combined with other renewable energy sources, holds immense promise for a wide range of applications. Solar radiation is quickly gaining popularity as a viable alternative to finite nonrenewable energy sources. The electromagnetic radiation emitted by the sun includes radio waves, infrared, visible, and ultraviolet light, as well as X-rays and gamma rays.[1–4]

The conversion of renewable solar energy into any useful form involves several steps. There are numerous losses in the energy conversion process chain from basic energy carriers to ultimate energy usage[5,6]. For instance, large quantity of converted energy ends up as waste heat due to friction, which is frequently dumped into the environment. Such waste heat must be exploited to improve energy efficiency and reduce energy consumption.[7–9] Waste/process heat is an inevitable byproduct from various industries, mechanical devices as well as energy production systems. Therefore, proper utilization of this useless resource may circumvent the current energy deficit. So, our main source of heat after the sun is waste heat from different processes, here is a pictorial depiction of sources of heat.[10]

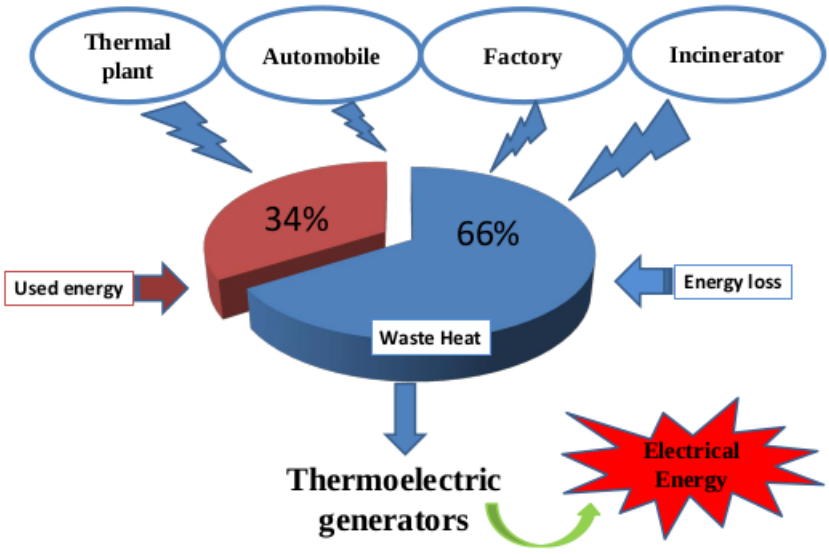

Figure 1.1:sources of Waste heat across the globe[10]

Automobile waste heat sources, and industrial waste are the big source of waste energy. Now let us discuss in brief the thermoelectric phenomena

1.1. Thermoelectric Phenomena

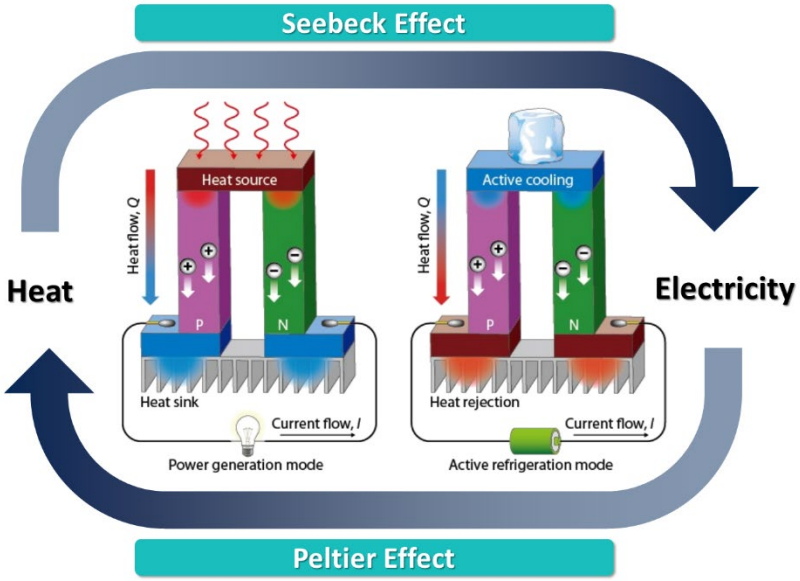

Figure 1.2:Thermoelectric phenomena for conversion of heat into electricity (Seebeck coefficient) and electricity into heat (Peltier effect)[11]

A thermocouple consisting of p-type and n-type materials coupled electrically in series and thermally in parallel is the simplest TE generator. Heat is applied to one side of the pair (the hot side), and a potential difference equivalent to the difference in temperature among the higher and lower temperature ends is created when negative/positive carriers migrate to the lower temperature side. A TE cooler (Peltier effect) is also depicted in this diagram, which turns the potential difference into a temperature gradient. An electrical current is formed when a voltage is applied to the electrodes, and thermal energy is transmitted in the direction of the carriers of the charge[11–13].

1.1.1. Strategies to develop potential thermoelectric material

To develop novel, low-cost, environmentally friendly, and high-efficiency TE materials, a further in-depth scientific study will be necessary. Currently, thermoelectric investigation is being done in two different ways: one is looking for novel high-efficiency bulk compounds, and the other involves altering available compounds at the Nano level to minimize the phononic and electronic thermal conductivity and so attain high efficiency. Quantum confinement is achieved by decreasing the aspects from 3d (bulk) to 2D layered (Nano sheets) and 1d (wires)). Grain boundaries have a significant influence on lowering thermal conductivity, which leads to better TE characteristics (lower thermal conductivity and higher Seebeck coefficient).

1.1.2. Advantages and disadvantages of thermoelectric devices

The benefits of TE generators/refrigerators over conventional technologies are discussed below[14,15]:

1. No mechanical moving components -which means minimal maintenance.
2. Compact and light weight – convenient in terms of size and weight
3. capable of working in both cold and hot environments,
4. Ecofriendly - No harm for the environment
5. Capable of re-purposing waste heat

When compared to conventional devices, TE devices have a poor conversion efficiency (about 12 percent). The efficiency of environment friendly TE materials is needed to improve.

1.1.3. Uses of Thermoelectric materials

thermoelectric materials have wide range of applications in industries as well as in the missions of space which may last weeks and require a constant source of electricity. In industries, process/waste heat at relatively high temperature can be useful for conversion and/or storage purposes. Solar energy is also another efficient source of heat for producing electricity, but its temperature needs to be raised appreciably for useful work. Approximately ¼th part of the intake energy is turned into mechanical movement in a conventional gasoline-powered combustion engine. The fact that exhaust gas has a higher temperature, the effective temperature for TE conversion is lower due to difficulty in gathering it. Even a slight temperature differential between the cold and hot sides can create electricity. The air conditioning system may make use of this electrical energy. In summer and winter, it is used for cooling and heating seats respectively. All electronic gadgets produce waste heat, which must be quickly dissipated in surrounding environment for proper functioning of the devices. Only TE technology can provide quick cooling to devices while operating silently, unlike traditional systems. For example, TE cooling has been used to improve the operation of electronic microprocessors like as central processing units in computers. Current TE devices, however, do not perform well enough because of their poor efficiency. Single layer-based TE devices are used to operate the diodes at same temperature, allowing the wavelength to be stabilized. When the efficiency of TE technology reaches that of traditional mechanical applications, it will have a bigger commercial market, it may become feasible, displacing current systems that release greenhouse gases. With increasing temperature, the speed and working life of many electrical equipment (circuits) reduces progressively. As a result, effective thermal management is a critical component in determining the performance and longevity of electronic equipment. Peltier coolers might function more efficiently if ZT value of 2 is obtained, providing more cooling with less electric power input. Steel, cement, Aluminum, and glass production industries are dependable sources of wasted heat [95]. It may be installed in car or home window to generate electrical energy. Success in improving the efficiency of TE materials, based on these factors, might update the cooling and electrical energy industries[16,17].

1.1.4. Merits and Demerits

As opposed to traditional fossil generators, one of the key advantages of employing TE devices is that it uses waste heat, which is released to the surrounding environment, thus raises the temperature of earth. Furthermore, as TE devices have no moving or mechanical parts, they can operate for an extended period of time without a need to be repaired. moreover, the absence of moving parts ensures that these gadgets are exceptionally silent and participate in noise pollution reduction. Also there are no harmful bi-products, such as harmful gases, which is also good for the environment. The biggest disadvantage of TE devices is that they are bulky. Nevertheless, TE materials offer many advantages and pledge to be viable as compared to existing materials[11].

Theoretical Background

To analyze the results, we will go through some basics of energy band structure and DOS in electronic properties and absorption of photons in the semiconductor materials in optical properties. To discuss the result, first of all, l will skim through the fundamentals of band structure, the density of states, and electronic characteristics of different optical terminologies such as absorption dielectric function, refraction, and reflection. In the electronic section, we will cover Bloch's theory, both spaces real and reciprocal, l and band structures.

1.2. Electronic Properties

1.2.1. Bloch Theory

As we have seen above, the problem of solving Schrodinger equations for N-interacting particle system is reduced to N-non interacting particle system with Kohn-Sham equations but still, this is an enormous task to solve this problem.

As discussed earlier the many-body problem has been reduced to N non-interacting particle system, but this simplification is still not enough to make it simpler we move forward to Bloch theory[18,19]. It is precisely applicable to repetitive systems.

This theory works only for systems that do not interact and are static in potential. This theorem for the translatory symmetric system and having, the static potential can be defined as

$$V(r) = V((r + R))$$

It simply defines the system as potential in a crystal is repetitive so the probability of locating the electron is repetitive and so the wave function is supposed to be repetitive which is given as:

$$\psi_{(r)} = u_k(r)e^{ik.r}$$

It is the product of the repetitive function of the crystal $u_k(r)$ and the function of plane wave $e^{ik.\,r}$. using repetitive property of the function, we get

$$u_k(r + a) = u_k(r)$$

The above equation shows the periodic function where 'a' is the interatomic spacing, using repetitive property wave function is given as

$$\psi_{(r+a)} = e^{ik.a}\psi_{(r)}$$

And the mathematical form of $u_k(r)$ is given as

$$u_k(r) = \sum_G C G_K e^{iG.r}$$

Where G is the reciprocal lattice vector

1.2.2. Reciprocal Lattice Space

The Fourier transform of real space is called reciprocal space having corresponding periodic reciprocal lattice[20], so the domain of the k space is supposed to be real space. The lattice vectors in real is given as

$$r = xa + yb + zc$$

The reciprocal lattice vectors, having $a*$, $b*$, $c*$ unit vectors, in momentum space k is given as

$$G = ma^* + nb^* + oc^*$$

1.2.3. First Brillion Zone

The Brillion zone is of utmost importance and helps a lot in defining the band energy theory. The first Brillouin zone is also termed the Wigner-Seitz cell of the k lattice. It is the locus of positions that are nearest to the lattice positions at the origin than to any other position[21]. It contains a k vector which is very vital in defining the band structures. It is fundamentally explained as a primitive cell. In a similar way, the real space is segmented into the 'Wigner Seitz cell', the k space similarly is segmented into Brillion zones. It tells about the k space lattice vectors in momentum space k. For instance, if we take the First Brillouin zone as a cube the it is convenient to make primitive lattice because the special positions in the first Brillion zone are convenient. The reciprocal lattice vectors with special positions for simple cubic primitive cells are written as follows

Table 1.1:Reciprocal lattice vectors for cubic cell[21]

Label	**Coordinates of simple primitive cell**	**Coordinates in *k space***
Γ:	*(0a∗+0b∗+0* c∗)	((0k_x *+0*k_y+0k_z)
X:	*(1/2a∗+0b∗+0*c∗)	((π/a) k_x *+0*k_y+0sk_z *)*
M:	*(1/2a∗+1/2b∗+0*c∗)	((π/a) k_x *+(π/a)* k_y+0k_z *)*
R:	*(1/2a∗+1/2+b∗+1/2* c∗)	((π/a) k_x*+(π/a)* k_y+(π/a) k_z*)*

1.2.4. Tight Binding Model

In this model, the wave-functions of atoms placed on each lattice site are superimposed on each other. Atomic orbitals are employed as basic wave-functions in the tight wave functions.[22] The electrons are bonded to their atoms and become delocalized as we move closer to them. Let's look at an example of a diatomic molecular system with specified energy levels that forms a molecule when brought close together, as shown in the given Figure. Both atoms' energy levels are combined to form molecular orbitals. Because the potential of both atoms altered as the molecule formed, the energy levels were divided up. The anti-bonding orbital is on the top level, whereas the bonding orbital is on the lower level.

Now assume eight atoms creating a similar molecular structure, with their energy levels divided up as shown in Figure below. We'll have these levels all over the place as we bring more and more atoms together. As a result, the graphic above depicts the entire energy band diagram. As a result, in solids, there exist large number of closely spaced atoms, and each atom fragments into N-closely spaced sub levels. The number of atoms in a solid is represented by the letter 'N.' When there are 10^{23} atoms in a solid, their sublevels are so close together that they appear to form a continuous energy band.

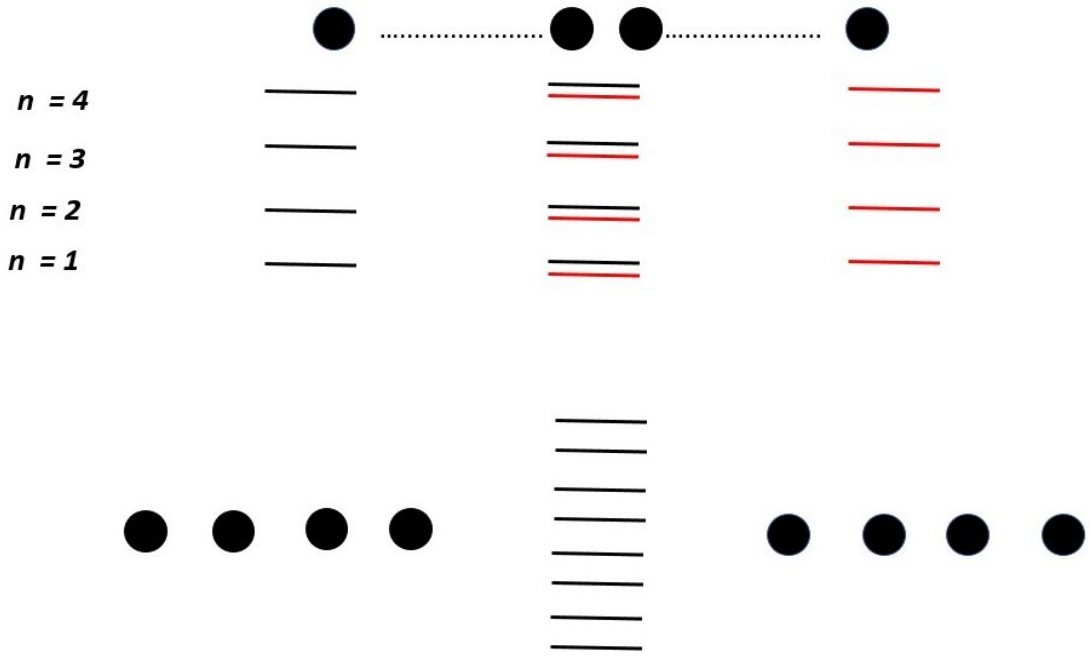

Figure 1.3:Energy levels division[22]

The space between two energy bands is referred to as the band gap since each excited band forms a band. This region is also known as the prohibited energy band gap, which essentially implies that the electros cannot occupy it. Bandwidth or dispersion is one of the most noticeable characteristics of the bands. This is the energy differential between the band's peak and lowest positions. The higher the energy band, the wider it is, since higher energy states relate to larger atomic radius, it causes more power perturbation, which is the primary cause of energy level splitting. Linear Combination of Atomic Orbitals is the first quantum mechanical model utilized to solve the problem of localized electrons in a system of two atoms (LCAO). The molecular orbital of a two-electron system may be represented as the sum of the atomic orbitals of two atoms.

$$\Psi molecule = a\phi atom1r + b\phi atom2\, r$$

The coefficients for atom 1 and atom 2 are a and b, respectively.
where a and b are having values of 1 in a homonuclear molecule. For the criterion that the wave function must meet the Bloch theorem, we may now build a crystal wave function or crystal orbital for an electron using LCAO. The LCAO approach works well with localized electrons but not with delocalized electrons. We can describe the band structure of most crystals and metals using this approach.
The wave function for a group of atoms in a crystal will be expressed as follows:

$$\Psi kx = \sum_{-\infty}^{\infty} n = e^{iknа}\phi atoms\, x - na$$

Where 'na' denotes the atom's location.

We may write the above equation as follows to fulfill the Bloch theorem:

$$\Psi kx + a = \sum_{-\infty}^{\infty} n = e^{ikna} \phi atoms\, x - na + a$$

If we solve the above equation, we get the result in the form:

$$\Psi_{kx} = e^{ikna}\, \Psi_{kx}$$

Bloch's equation is satisfied by the above given solution. This suggests that the wave function of a linear combination of atomic orbitals' approximation. As a result, the energy of atomic orbitals corresponding to this wave function may be used.

The energy has the following form:

$$Ek = \Psi_k H \Psi_k$$

The tight-binding model is a technique for calculating electronic band structures in metals and crystals. Formation of electronic band structures. Let's look at how the tight-binding model aids in the formation of the band structure. The most basic three-dimensional substance is alpha polonium (Po), often known as primitive cubic metal or simple cubic metal. The predicted band structure for Po with the simple cubic structure is shown below. We'll use DFT calculations to interpret the peaks in this section. The dotted line will be set to zero energy, which is known as Fermi energy. Each unit cell has one Po atom, which is a 'p' block atom. It possesses one valence shell' and three 'p' orbitals (6s and $6p_x$, $6p_y$, and $6p_z$). In the energy band diagram, we would see a total of four bands.

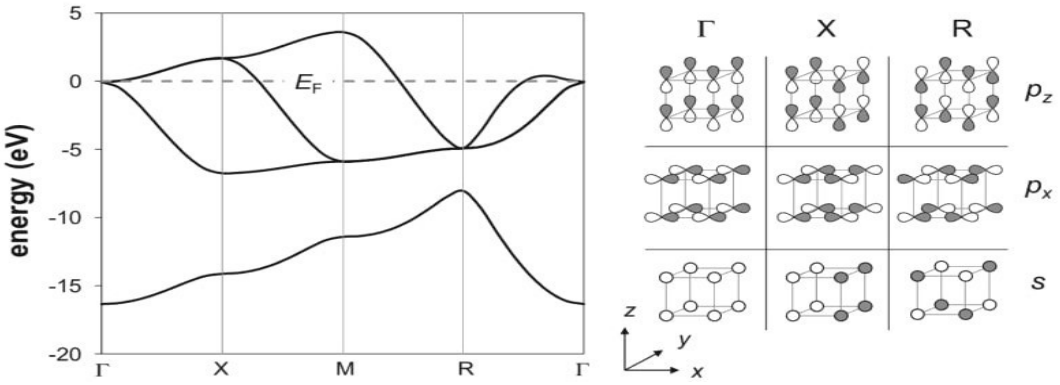

Figure 1.4:Orbital overlap and band positions

The 6s orbital overlap is shown by the first peak. When we move from one-unit cell to the next, all of the atoms have a similar phase. The basis set is a single atomic orbital in this case. In above given figure, all of the atoms are connected by 6 closest neighbor bonding atoms. As a result, the energy level is relatively low at this position. The phases of the orbitals will alter along the x-axis as we go from point Γ to X which indicates that there are more bonding orbitals than anti-bonding orbitals, therefore the net energy is still bonding but greater than the Γ point. When we translate the unit cell to point 'M,' the phases of the orbitals will shift once more. The four closest atoms in the 'XY' plane are anti-bonding, whereas the two closest neighbors in the 'z-direction are bonding, resulting in a net anti-bonding orbital that is greater than the bonding orbitals. The highest energy crystal orbital in the 6s band is point 'M,' where all six closest neighbor interactions have become anti-bonding. Fermi level cuts 6p orbitals because they are two-third occupied. The atomic orbitals associated with 6s, 6px, and 6pz at the X and R points are degenerate, as shown in Figure above. All 6p bands create a σ-antibonding connection with two nearby atoms and a c-bonding interaction with the remaining four atoms at this point. At R, the σ-bonding interaction takes precedence over the π-antibonding interaction. Because all interactions are bonding, the 6px band at X achieves the minimal level. At the X point, however, the 6py and 6pz display substantial σ-antibonding with their closest neighbors. As a result, the energy of 6py and 6pz is substantially higher than 6px at this point.

1.3. Optical Properties:

1.3.1. Introduction

Light has a variety of interactions with matter. Optical characteristics are described as a substance's reaction to electromagnetic radiation, and optical materials are substances whose properties may be influenced by the light flow. Every substance has its unique optical qualities; some absorb various colors, while others reflect and scatter light in various ways. Metals, for example, are gleaming water, whereas glass is clear. Metals reflect all wavelengths up to ultraviolet; insulators are dielectrics that are transparent to visible light, and semiconductors are often opaque to visible light but transparent to ultraviolet light[23–25]. The optical qualities of a substance are governed by its structural properties and chemical composition, which varied from one material to the next. Solid-state optical characteristics may be used to compute energy band structure, impurities, defects, and lattice vibrations. The nature of absorption, reflection, and transmission will be briefly reviewed in this section. When incoming light strikes a medium, reflection, propagation, and transmission are some of the main processes that may be seen[23].

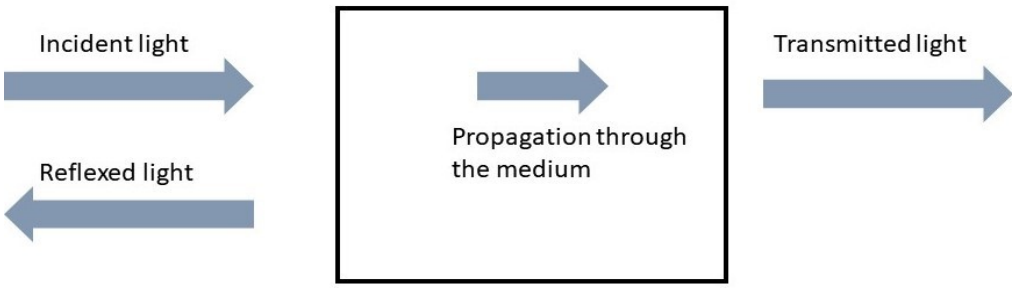

Figure 1.5:Depiction of light transmission and reflection

A few incident lights reflect some propagate, and some transmit via the optical medium, as seen in this illustration66. The relationship between optical absorption and absorption coefficient will be discussed first. After that, we'll look at complex dielectric functions and optical conductivity, as well as the relationship between solids' energy band structures.

1.3.2. Optical absorption

Optical absorption refers to the material's absorbing of light's electromagnetic radiation. It is determined by the material's nature. When the frequency of light approaches the natural resonance frequency of dipole oscillators, absorption occurs. As a result, the dipole oscillators absorb only a fraction of the energy of input electromagnetic light, and the remainder is wasted as heat. Figure below shows an example of this. The valence band's energy is E_v, the conduction band's energy is E_c, and the bandgap energy is E_g. When a photon with the incident energy hf collides with the substance, two processes can occur[26,27]:

1. When hf is larger than E_g, the electron in the valence shell absorbs energy and becomes excited. This electron moves from the lower energy level to the higher energy level. In the valence band and conduction band, the electron-hole pair is now formed. Due to scattering, the excited electron now loses energy to the lattice. The electron now goes from the conduction band to the valence band, where it recombines with the hole.
2. There is no excitation process if hf is smaller than Eg. As a result, some materials are transparent within a specific wavelength range.

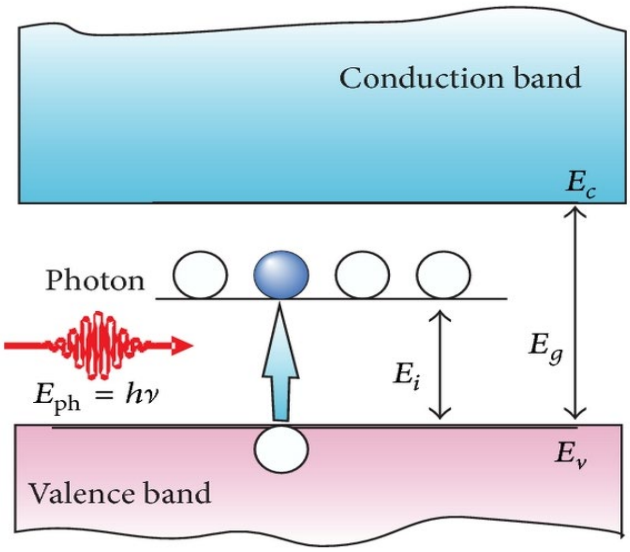

Figure 1.6:Excitation of electron after photon absorption

Now we'll calculate the absorption coefficient and examine how it relates to the absorption process itself[28].

1.3.2.1. Absorption coefficient

An absorption coefficient α is a measurement of how much light is absorbed by an optical material. It's defined as the percentage of energy absorbed per unit length of medium. If incident light from a monochromatic source fall on the optical medium. If hf is bigger than Eg, a portion of the photon's energy is absorbed by the substance, while the remainder is transmitted. If the beam propagates in the x-direction and the intensity of position at 'x' is I(x), then the intensity decreases in an incremental slice of thickness dx as follows[29,30]:

$$I(x) \propto -\left(\frac{dI(x)}{d(x)}\right)$$

$$I(x) = -\alpha \frac{dI(x)}{d(x)}$$

Equation has the following solution:

$$I(x) = Ioe^{-\alpha x}$$

The intensity of the light hitting on the substance is measured in Io. Similarly, the residual intensity of the transmitted light after incident light passes through the medium may be stated as:

$$It(x) = Ioe^{-\alpha x}$$

$$It(x)Io = e^{-\alpha x}$$

With the graph below, we can observe how the optical absorption coefficient (α) changes as a function of photon energy.

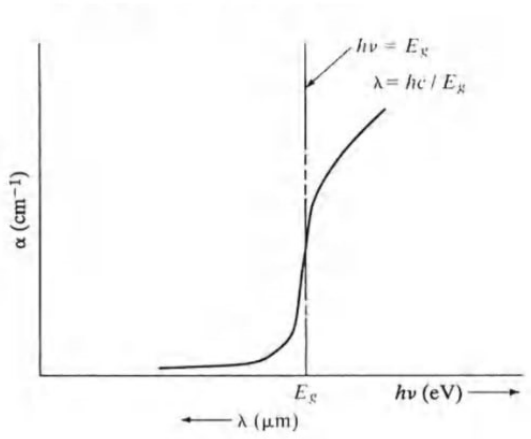

Figure 1.7:Energy vs optical absorption graph

The value in the first section of the Figure shown above is pretty small, indicating that the sample transmits the majority of the light. At these frequencies, the sample is transparent (hf is less than Eg). The energy of a photon becomes equal to the energy of a bandgap in the second area, and the value of α increases fast in this section. In the third zone (when hf is greater than or equal to Eg), because the photon has more energy, it will disrupt covalent bonds and generate an electron-hole pair. The value of α is quite high at this spot, and the material is opaque to incoming light.

1.3.3. The complex dielectric function and complex optical conductivity

Maxwell equations give birth to the concepts of the complex dielectric function and optical conductivity[31,32]:

$$\nabla^2 E = \frac{\varepsilon\mu}{c^2}\,\frac{\partial^2 E}{\partial t^2} + \frac{4\pi\sigma\mu}{c^2}\,\frac{\partial E}{\partial t}$$

$$\nabla^2 H = \frac{\varepsilon\mu}{c^2}\,\frac{\partial 2H}{\partial t2} + \frac{4\pi\sigma\mu}{c^2}\,\frac{\partial H}{\partial t}$$

The quantity in the previous equations introduces the notion of the complex dielectric function. In order to solve equations above, we need a sinusoidal solution.

$$E = Eoe^{-i(K.r-\omega t)}$$

K is the complex propagation constant, and ω is the light's angular frequency. To solve above given equation for H, a similar wave solution is required. The wave vector is represented by the real component of K, whereas the imaginary part shows wave attenuation in solids. If we substitute solution of our equation for the value of the wave vector in the given equation, we get the following expression:

$$-K^2 = \frac{-\varepsilon\mu\omega 2}{c^2} - \frac{4\pi i\sigma\mu\omega}{c^2}$$

The second expression of equation above vanishes if there is no attenuation in solids, then the equation above becomes:

$$K0 = \frac{\omega}{c}\ \sqrt{(\varepsilon complex\ \mu)}$$

ε is however a real function of K, it also contains a loss factor, therefore the dielectric function may be represented as follows in terms of real and complex parts:

$$\varepsilon complex = \varepsilon + \frac{4\pi i\sigma}{\omega} = \varepsilon 1 + i\varepsilon 2$$

$$\varepsilon complex = \frac{4\pi i\sigma}{\omega} + \frac{\varepsilon\omega}{4\pi i}$$

We may define complex conductivity using equation above:

$$\sigma compelx = \sigma + \frac{\varepsilon\omega}{4\pi i}$$

Now that we've established complex conductivity (complex) and dielectric terms (complex)[33–35], let's move on to the next step. The refractive index is closely connected to dielectric characteristics and permittivity. The effect of radiation on matter is described by the dielectric constant, permeability, and conductivity. Because light is a transverse wave, there are two feasible orthogonal directions for the E vector in a plane perpendicular to the propagation direction, and the polarization of light is determined by these directions.

1.3.4. Complex Refractive Index

The refractive index is a combination of real and imaginary parts and is wavelength dependent and may be represented as follows:[36,37]

$$Ncomplex = \sqrt{\mu\varepsilon complex}$$

The relationship between the K and N complex may be described as follows:

$$K = \frac{\omega}{c} Ncomplex$$

Now we will write N complex in terms of real and complex function

$$Ncomplex = n + ik$$

The optical constants for solids are n and k, where n is the refractive index and k is the extinction coefficient. The refractive index can reveal a lot more about a material's optical characteristics. The real component of the refractive index indicates the change in wavelength or velocity of a wave as it transitions from vacuum to medium, whereas the imaginary part depicts the wave's attenuation in the medium.

1.3.5. Reflectivity

Reflectivity is a material attribute that indicates how much light is reflected off the material's surface in relation to the amount of incident light. Prior given Figure shows a schematic of the optical system[38]. We assumed that the material in Figure is thick enough to absorb light. If we omit the reflection from the rear of the material, the one-dimensional propagating wave may be expressed as[39]

$$Ex = Eoe^{-i(K.r-\omega t)}$$

In equation above, K is the complex propagation constant, which has previously been determined. Both incident and reflected waves exist in free space:

$$Ex = E1e^{-i(\omega zc-\omega t)} + E2e^{-i(-\omega zc-\omega t)}$$

The continuity of Ex may be connected to the following equation using equations given above

$$E0 = E1 + E2$$

We may get the following relationship from the Maxwell relation:

$$\frac{\partial Ex}{\partial z} = \frac{i\mu\omega}{c} Hy$$

Using equations above, we get

$$E0K = \frac{E1\omega}{c} \ \frac{-E2\omega}{c} = \frac{E0\omega}{c} Ncomplex$$

$$E1 - E2 = E0Ncomplex$$

R is now defined as the perpendicular incident reflectivity.

$$R = \frac{E2^2}{E1}$$

We are now familiarizing with reflection coefficient r given by

$$r = \frac{E2}{E1}$$

The following are the outcomes of above equations

$$E2 = \frac{1}{2} E0\ 1 - Ncomplex$$

$$E1 = \frac{1}{2} E0\ \big((1 + Ncomplex)\big)$$

The perpendicular incident reflectivity has now obtained the form

$$R = \frac{1 - N_{complex}^2}{1 + Ncomplex} \quad = \frac{((1-n)^2 + k^2\ )}{(1+n)2 + k2}$$

Another significant optical constant termed reflectivity R has now been added. The following relationship may now be used to calculate the power transmitted or absorbed by the material at perpendicular incidence.

$$1 = A + R + T$$

When incident light passes through the optical medium, four processes can occur. Some light is absorbed by the material, some are reflected at the material's surface, some is scattered in various

directions, and some are transmitted through the sample. Optical coefficients, which reveal macroscopic features of the material, characterize all of these activities. The dielectric constant was discussed in relation to optical conductivity and physical observables in the previous section. Optical properties play a crucial part in electronic energy band operations when treating a solid. We'll look at several sorts of energy bands in optical characteristics in the next section.

1.3.6. Direct and Indirect bandgap

In a direct bandgap, the lower part of the conduction band and the upper part of the valence band have the same momentum value. In this bandgap, the electron can directly emit a photon. The energy difference between the conduction and valence bands is the smallest in the direct band gap. For the Indirect band gap, the lower part of the conduction band and the upper part of the valence band must not exist at the same momentum value. At different momentum levels, the maximum energy of the valence band gap occurs[40,41]. Figure below depicts the direct and indirect band gap for semiconducting materials[41].

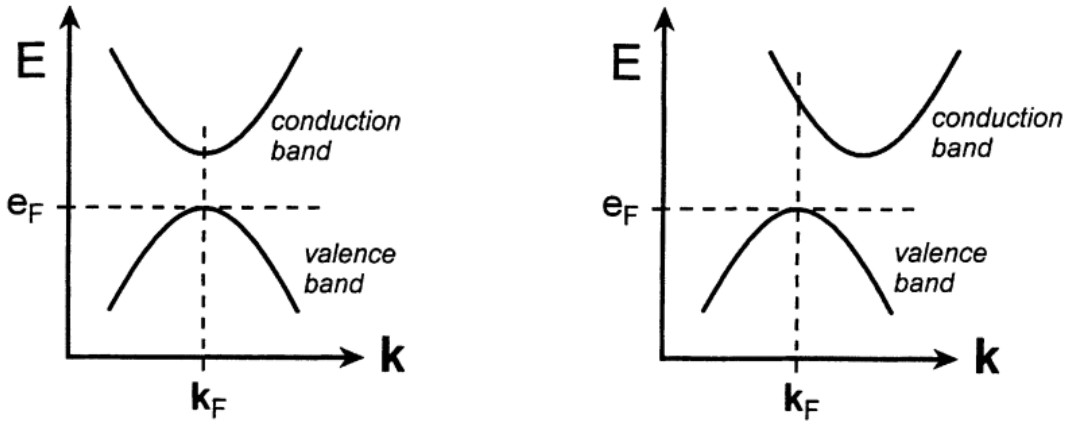

Figure 1.8:Direct band gap and indirect band gap diagram

1.3.7. Optical loss

Optical loss is a reduction in the intensity of light as it enters a medium.[42,43]

1.4. Thermoelectric Materials Modeling

Figure of merit, which is dependent on the material's transport coefficients, was detailed earlier. In the hunt for better thermoelectric materials, these coefficients must be fine-tuned. We'll now go through how these coefficients were calculated using the findings of our first-principles band structure calculations. Electrical (E) or thermal currents (JQ) are induced in the system when there is perturbation in an electronic field or a temperature difference the following are the relationships between the electronic field (E) and the temperature difference (T), as well as the accompanying J and J_Q for solids[44]:

$$\vec{J} = (\sigma\vec{E} - S\sigma\nabla T)$$

$$\vec{J_Q} = (S\sigma T\vec{E} - (\kappa\nabla T))$$

If electrical current is zero, voltage difference in a material due to difference in temperature is measure of Seebeck coefficient.

1.4.1. Thermoelectric Properties using BoltzTraP:

To calculate the above-mentioned transport coefficients, we'll require a microscopic model of the transport process. In the constant relaxation time approximation, we will apply the semi-classical technique provided by the solution of the Boltzmann transport equation. The electric current of carriers is defined as follows[44]:

$$J = e \sum_k f_k V_k$$

, where e denotes the carriers' charge. vk is the group velocity associated with the quantum state labelled with k, and fk is the population of that state.

$$V_k = (\frac{\partial w}{\partial k})$$

The distribution function fk is used to calculate the number of carriers in the state k in the locality of r. The distribution function can be affected by diffusion, outside fields (such as magnetic and electric fields or a temperature difference), and carrier scattered by phonons or localized scattering sites (such as impurities or crystal defects). The population of the state k is the solution of Boltzmann's equation, which includes the interaction of all of the mechanisms outlined above:

$$\frac{\partial f_{\vec{k}}}{\partial t} + \vec{v}_{\vec{k}} \,.\, \nabla_{\vec{r}} f_{\vec{k}} + \frac{2\pi e}{h} \left(\vec{E} + \frac{1}{c}\, \vec{v}_{\vec{k}} \times \vec{H}\right).\, \nabla_{\vec{k}} f_{\vec{k}} = \left(\frac{\partial f_{\vec{k}}}{\partial t}\right)_{scattering}$$

The Fermi-Dirac distribution function f0 (k) is the stationary solution of the Boltzmann's transport equation for fermions in the absence of fields. In the absence of magnetic fields and temperature gradients, linearizing the preceding equation and applying the relaxation time approximations for the scattering term, the population is

$$f_{\vec{k}} = f_0(\vec{k}) + e \left(-\frac{\partial f_0(\vec{k})}{\partial \in_{\vec{k}}}\right) \tau_{\vec{k}} v_{\vec{k}} \vec{E}$$

The Fermi-Dirac distribution is the electron equilibrium distribution.

$$f_0(\vec{k}) = \frac{1}{\exp\left(\frac{\in_{\vec{k}} - \mu}{K_B T}\right) + 1}$$

μ is the chemical potential, which is greatly influenced by carrier concentration and only moderately by temperature.

Under the BoltzTraP program[45], in the so-called constant scattering time approximation, $\tau_{\vec{k}}$ will be kept constant. The code uses a Fourier expansion of the band energies acquired from the WIEN2k calculation, allowing the velocities to be calculated as Fourier sums that can be evaluated quickly using rapid Fourier transformation. The conductivity tensor may be represented as using the aforementioned relation for fk to compute the current.

$$\sigma = e^2 \sum_k \left(\frac{-\partial f_0(\vec{k})}{\partial \in_{\vec{k}}} \right) \tau_{\vec{k}} v_{\vec{k}} v_{\vec{k}}$$

Once we know the transport distribution, we can directly compute the coefficients of transport used in the figure of merit. We've got conductivity

$$\sigma = e^2 \int \left(\frac{-\partial f_0(\vec{k})}{\partial \in_{\vec{k}}} \right) \tau_{\vec{k}} v_{\vec{k}} v_{\vec{k}} \; d \in_{\vec{k}}$$

Seebeck can be calculated using

$$s = \frac{e}{T \sigma} \int \tau_{\vec{k}} v_{\vec{k}} v_{\vec{k}} \left(\frac{-\partial f_0(\vec{k})}{\partial \in_{\vec{k}}} \right) \left(\in_{\vec{k}} - \mu \right)^2 d \in_{\vec{k}}$$

And here is given thermal conductivity

$$K = \frac{1}{T} \int \tau_{\vec{k}} v_{\vec{k}} v_{\vec{k}} \left(\frac{-\partial f_0(\vec{k})}{\partial \in_{\vec{k}}} \right) \left(\in_{\vec{k}} - \mu \right)^2 d \in_{\vec{k}}$$

Under the constant relaxation time condition, the Seebeck coefficient and dimensionless thermoelectric figure of merit are independent of$\tau_{\vec{k}}$. This is why, when analyzing the

transportation, these parameters will be our primary emphasis. This form of computation necessitates a highly dense k-point sample, well above that required for a self-consistent calculation. In various circumstances when the transport coefficients may be compared to actual data, the Boltzmann transport theory has been shown to be correct.

Electronic power factor is given as

$$Power\ Factor\ =\ S^2\sigma$$

Figure of merit is given as

$$ZT\ = \frac{\mathrm{S2\sigma T}}{(\mathrm{Kelectronic+Klattice})}$$

1.4.2. Figure of Merit and Efficiency

A TE material's maximum efficiency is determined by (1) the Carnot efficiency term (which cannot be exceeded) and (2) a term characterizing the TE characteristics (S, σ, and τ). The figure of merit takes the form

$$zT = \frac{S^2\sigma T}{\kappa}$$

Where σ electrical conductivity (1/cm), S = Seebeck coefficient (V/K), and T = temperature

Furthermore, κ is the thermal conductivity (W/cm K), which is further separated into contributions from the lattice (l) and electronic (e) components, (κ = κ l +κ e) (more about this is discussed in the following segment).

List of some famous thermoelectric materials is given below[11]

Table 1.2:Table of high ZT value materials

Compound	Chemical formula	zT	T
Bismuth Telluride	Bi_2Te_3	0.6	400
Lead Telluride	PbTe	0.8	773
TAG-85	$(AgSbTe_2)_{0.15}(GeTe)_{0.85}$	1.4	750
Cs-Bismuth Telluride	$CsBi_4Te_6$	0.85	255
Clathrate-1	$Ba_8Ga_{16}Ge_{30}$	1.35	900
La-Skutterudites	$LaFe_3CoSb_{12}$	1.40	1000
LAST	$AgPb_mSbTe_2$	1.7	700
SALT	$NaPb_mSbTe_{2+m}$	1.6	675
LASTT	$Ag(Sn,Pb)_mSbTe_{2+m}$	1.4	700
Zinc Antimonide	β-Zn_4Sb_3	1.3	660
Silicon Germanium	$Si_{1-x}Ge_x$	0.9	900
Mo-Antimonide	$No_{0.06}Mo_3Sb_{5.4}Te_{1.6}$	0.93	1023

In order to produce a high figure of merit, the TE material must have both a good electrical and a poor thermal conductor, as well as have a high Seebeck coefficient. Increasing σ via increasing the carrier concentration, on the other hand, typically lowers S and increases κe. As a result, controlling the numerator $S^2\sigma$ (the power factor) and the denominator κ separately is a top priority. Because phonon scattering is enhanced and thermal conductivity is lowered, alloying, vacancies, and the application of strain are effective and often used techniques to improve TE characteristics.

S, σ, $S^2\sigma$ and κ and as a function of free-charge carrier concentration in the following figure[11].

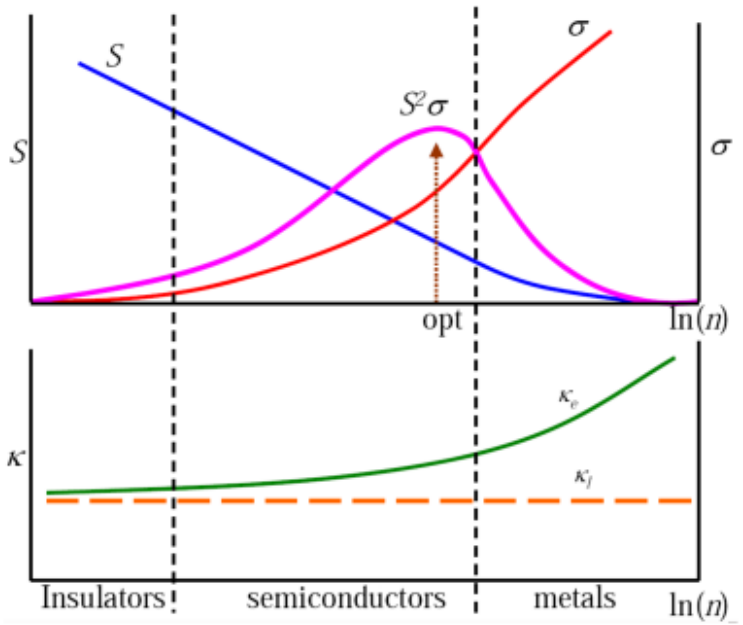

Figure 1.9:Comparison of thermoelectric properties of insulators, semiconductors and conductors

Because of their low Seebeck coefficient and substantial electronic contribution to heat conductivity, metals are poor TE materials. Insulators have a low electronic contribution to heat conductivity and a high Seebeck coefficient. Their charge density is minimal, resulting in limited electrical conductivity and a low TE effect. Semiconductors with an electrical density of roughly 10^19/cm^3 83, as shown in the figure and the table, are the best materials. The Seebeck coefficient decreases as the carrier concentration grows from insulator to semiconductor to metal, as seen in Figure 1.3. Electrical conductivity behaves in the opposite way. It is necessary to choose the best figure of merit where both lines meet in order to arrive at the best figure of merit. It is also obvious that a reduction in electronic thermal conductivity would result in a reduction in electrical conductivity and, as a result, a reduction in the figure of merit. Furthermore, at an optimal carrier concentration of 10^19 cm^{-3}, the contribution of lattice thermal conductivity is smaller than the electronic component. As a result, doping would have a favorable effect on the figure of merit up

to a certain carrier concentration. The figure of merit might be enhanced even further by lowering the lattice thermal conductivity without affecting the other factors.[11,46]

Table 1.3:TE properties of metals, semiconductors and insulators at room temperature

Properties	Metal	Semiconductor	Insulator
S (μVK^{-1})	~ 5	~ 200	~ 1000
σ (1/Ω cm)	~ 10 6	~ 10 3	~ 10 −12
Z (K^{-1})	~ 3×10 −6	~ 2×10 −3	~ 5×10 −17

A TE device's figure of merit is calculated as follows:

$$ZTavg = \left(\frac{Sh - Se}{\sqrt{\frac{\kappa h}{\sigma h}} + \sqrt{\frac{\kappa e}{\sigma e}}} \right)^2 Tavg$$

Hole and electron doping are represented by h and e, respectively. The mean system temperature is T avg. The temperature differential and the material parameter ZT_{avg} have a direct impact on the device's performance. The Carnot efficiency defines efficiency as follows:

$$\eta = \frac{\Delta T}{Thot} \left(\frac{\sqrt{1 + ZTavg} - 1}{\sqrt{1 + ZTavg} + \frac{Tcold}{Thot}} \right)$$

1.4.3. Seebeck Coefficient

The induced TE voltage in consequence to a temperature differential across a material is measured by the Seebeck coefficient (or thermo power) S of the material. We've got

$$S = \frac{K_B}{e\sigma}\int_0^{\infty} \sigma(e)(\frac{E - E_F}{K_B T})(\frac{\partial f_o(E)}{\partial E})dE$$

The Boltzmann constant, electron charge, electrical conductivity, Fermi energy, and Fermi distribution function are kB, e, E F, and f0 correspondingly. The last equation reduces to in the case of metals and degenerately doped semiconductors.

$$S = \frac{\pi^2 K_B^2}{3e}(\frac{d\{\ln[\sigma(E)]\}}{dE})$$

It has a wide range of validity.

1.4.4. Electrical Conductivity

The ability of a material to allow charge carriers (electrons or holes) to travel move in its crystal lattice is given by its electrical conductivity (σ). In this theory, it is computed, using the relation between charge carrier density (n) and carrier mobility (μ).

$$\sigma = n\mu e$$

$$\mu = \frac{e\tau}{\mathrm{m}^*}$$

Relies on the carrier's effective mass m, which is directly connected to the band dispersion86and the relaxation/scattering period (time between carrier collisions). The drift velocity is dictated by

the relaxation/scattering time, which is the amount of time the carrier is propelled by the electric field before colliding and changing its direction and/or energy.

Ionized impurities, neutral impurities, electron-phonon interaction (acoustic phonon scattering, optical phonon scattering, and piezoelectric scattering), and electron-electron contact are all sources of scattering in semiconductors. The contributions of the various scattering effects are added together to get the overall mobility.

$$\frac{1}{\mu_{Total}} = \frac{1}{\mu_{Ionized}} + \frac{1}{\mu_{Neutral}} + \frac{1}{\mu_{el-ph}} + \frac{1}{\mu_{el-el}}$$

Ionized impurity scattering occurs when an electron or hole approaches an ionized impurity and is deflected by Coulomb forces.

The amount of deflection is determined by the carrier's velocity and closeness to the ion. Because the collision probability is higher in strongly doped materials, the mean free time between collisions and consequently mobility is reduced. In ionized impurity scattering, mobility is linearly proportional to temperature, $\mu \propto T^{3/2}$. At low temperatures, scattering due to unionized donors in semiconductors becomes dominant when carriers freeze out at the impurity surface (neutral shallow-level impurities). While mobility is formally independent of temperature, investigations demonstrate that many semiconductors have a modest relationship. Only at very high carrier concentrations (over $10^{19}/cm^3$) can neutral impurity scattering become significant. Electron-phonon scattering: In weakly doped or inherent semiconductors, the scattering of electrons by acoustic phonons is essential.

A deformation potential or piezoelectric scattering can cause an acoustical phonon to disperse.

On an atomic scale, the change in atomic spacing caused by the acoustic wave causes a change in the energy band gap. $T^{-3/2}$ is precisely proportional to the mobility owing to this deformation potential. Due to piezoelectric scattering, electron mobility changes with $T^{-1/2}$. Electron-electron scattering: If the density of electrons is less than $10^{17}/cm\text{^}3$, they are termed non-interacting. Above this threshold, electron-electron scattering takes over.

1.4.5. Thermal Conductivity

When it comes to thermal conductivity,

$$\kappa = \kappa_e + \kappa_l ,$$

The heat transfer contributed by moving charge carriers is represented by the electronic contribution $\kappa_e = L\sigma T$. For metals and small band gap semiconductors, the Wiedemann-Franz law 88may be used to approximate this. According to the Wiedemann- Franz law, the ratio of a metal's thermal conductivity to its electrical conductivity is in direct relation to its temperature, i.e., $\kappa_e = L\sigma T$ is the Lorenz number, which Sommerfeld calculated theoretically for metals89 and strongly doped semiconductors. By simply considering σ, the Wiedemann-Franz law provides a good estimate of the electronic contribution.

1.4.5.1. The contribution of the lattice

The heat generated by lattice vibrations is denoted by l. (phonons). Using the kinetic theory of gases, l is determined by the material's specific heat (CV), the phonons' mean free path (l), and the speed of sound (v). The Debye model can be used to describe it.

$$\kappa_l = \frac{K_B}{2\pi^2 v}\left(\frac{2\pi K_B}{h}\right)^3 \int_0^{\theta/T} T \frac{x^4 e^x}{(e^x - 1)^2}\, dx,$$

Where $x = \omega/k_B T$, ω is the phonon frequency, kB is the Boltzmann constant, v is the sound velocity. The thermal conductivity is influenced by the following scattering mechanisms: (a) Standard and umklapp mechanisms, three-phonon scattering (or phonon-phonon scattering), (b) point defects, (c) electron-phonon scattering, and (d) grain boundary scattering.
As a result, the total relaxation time is equal to

$$\tau^{-1} = \tau_N^{-1} + \tau_U^{-1} + \tau_{PD}^{-1} + \tau_{EP}^{-1} + \tau_B^{-1}$$

Assuming that normal and umklapp processes dominate the un doped compound's lattice thermal conductivity, U is equal to

$$\tau_U^{-1} = \frac{1}{b_0}\frac{\pi}{4}\frac{K_B}{2\pi^2 v}\frac{K_B^3 T^3 (2\pi)^3}{h^3\theta^2}\frac{n^{2/3}\gamma^2}{M_{ave}\delta}x^2$$

where b0 = 3.04 10^7 s^{-3} K^{-3} is the Debye temperature, Mave is the average mass, γ is the Grüneisen constant, and δ is the atomic volume's cube root

We've got

$$\tau_N^{-1} = \frac{U}{N}\tau_U^{-1}$$

$$\tau_{PD}^{-1} = \delta^3\frac{\Gamma}{4\pi v^3}\omega^4$$

Where is the scattering parameter and is the scattering parameter? On a single atomic site {equation}, for impurity atoms. The fractional concentration of impurity atom I is given by fi while its mass is given by Mi.

Moreover,

$$\tau_{EP}^{-1} = \frac{E_d^2 m^{*3} v(2\pi)^4}{4\pi h^4 d}\frac{K_B T}{\frac{1}{2}m^* v^2}\left\{\frac{h\omega}{K_B T} - \left\{\ln\frac{1+\exp\left[\frac{\frac{1}{2}m^*v^2 - E_F}{K_B T} + \frac{h^2\omega^2}{8m^*v^2(2\pi)^2 K_B T} + \frac{h\omega}{4\pi K_B T}\right]}{1+\exp\left[\frac{\frac{1}{2}m^*v^2 - E_F}{K_B T} + \frac{h^2\omega^2}{8m^*v^2(2\pi)^2 K_B T} - \frac{h\omega}{4\pi K_B T}\right]}\right\}\right\}$$

The deformation potential is Ed, and the density is d. Finally, due to grain boundary scattering, the relaxation time is given as

$$\tau_B^{-1} = \frac{v}{l}$$

The average grain size length and drift velocity, respectively, are l and v.

Chapter 2

Literature Review

In this chapter we discuss the prior research carried out on Calcium Oxide (CaO).

Elisabeth A. Mikajlo et al[47], has carried out the research. The six oxides measured, and estimated band structures are described. Electron momentum spectroscopy has been used to measure band structures. Observations are matched to first-principles computations performed that use the DFT and HF methods within the linear combination of atomic orbitals assumption. The LDA, the generalized gradient approach, and a combined technique combining precise interchange are all characterized by three DFT functionals. In general, the predicted O 2p band gaps and O 2p bandwidths scale linearly with the under root of the oxygen to oxygen spacing. Such patterns can be seen in the experimental results as well. The oxygen 2p–2s band gap is routinely underestimated by about a significant margin in HF estimates. The functionals used can account for the observed band gaps, showing that characterization of exchanging gets increasingly significant as positive ion size grows. The oxygen bands are overestimated by HF and DFT computations, but DFT providing ever more precise estimates. As the scale of the cationic ion grows, both measured and computed bandwidths converge, suggesting the exchange-correlation impacts are becoming less significant as the metal ion gets bigger.

The findings of this study are based on a thorough examination of all six oxides that enables comparative evaluation of existing experimental and theoretical and is properly enforced to the entire collection of data. The advantage of the EMS method is that it can investigate the band structures of these insulators materials without even being constrained by observations of "special points" or the usage of mono-crystal material, unlike optically and photo- luminescence methods. modern ab initio approaches can be actually linked to test findings with the very simple extra level of spherically averaged computations over multiple crystallographic orientations. In this paper lattice parameters are reported using different correlation functionals, using functional it is reported 4.847,it is mentioned 4.699, 4.811, 4.783 for LDA, GGA, Hybrid respectively.

M A Bolorizadeh et al[48], have reported that on the EMS measured Ca 3s and 3p core levels in CaO as well as the entire energy-momentum resolved electronic structure of the valence band. Along with other

accessible experimental and simulation data, it has also been compared with experimental findings to band structures computed using the full potential linear muffin-tin orbital approach. In terms of the dispersion and EMD of such 3p semi-core level, there is strong overall consistency between measured and computed. Whether or not simultaneous scattering is modeled in the computed data, the measured bandwidth of 0.7 0.1 eV does not disagree with the LMTO bandwidth. The calculated Ca 3s-3p splitting of 18.8 0.2 eV agrees very well with the available XPS data.

R.C Whited et al[49]., have reported Thermo-reflectance spectra between 6 and 8 eV are shown. The spin-orbit splitting of the 0(2p) level at r and the positions of exciton—phonon structures are reported with better values. Support for the valence band spin's typical ordering to be reversed—orbit splitting—for Magnesium oxide is offered. The observations are addressed considering current theoretical formulations of the interplay between the exciton and phonon. Again, values of spectral characteristics and splitting show slight variability between runs. The spin—orbit exciton states at F are represented by extremes I at 6.932eV and II at 6.971eV. The k=0 LO phonon energy (w0 =70 meV) splits off the minima (III) at 7.002 and (IV) at 7.039 eV, respectively, and these are thought to correlate to exciton—phonon characteristics.

Kaili Wu et al.[50], carried out the research using sophisticated hybrid density functionals (along with Alkauskas' technique), they have solved the band edge problem. The defect formation energy is aligned using the finite-size correction approach (FNV). Based on density functional theory, the defect formation energies of oxygen vacancies in CaO crystals with various charge states (0, +1, and +2) are studied. We start by optimizing every structure. After that, the three charge state defects' structures are examined. Finally, they provide an exact description of the optical spectra for electron-phonon coupled F and F^+ centers. Inference that these techniques can be used to compute the optical spectra of point defects. In this letter, using a combination of the GGA-PBE at the semi local level and more sophisticated hybrid density functionals, we carry out precise calculations on the defect production energy within the domain of simulations. The band gap of the HSE adjustment, which we have determined, is in good agreement with the outcome of the study. Following structure optimization, it has been explained the distortion of the oxygen vacancy with three charge flaws. Additionally, in order to get the accurate, the defect formation energy, it has been implemented the finite-size alignment method (FNV). The finite-size adjustment ranges between 0.5 and 2.2 eV.

Z.P Chang et al.[51], shown in the research using UPS (ultrasonic pulse superposition) method has been to quantify the mono crystal elastic constants and their first pressure derivatives for the Rock salt oxides

CaO, SrO, and BaO. The pressure dependency was determined linear in the scale up to 10 kbar. This has been supported by both theory and experiment that positive ion size has major impact on the elastic properties.

By P. Suresh et al.[52], following research has been carried out. It has been possible to build a CaO super cell pure and with oxygen deficiencies. Its structural, electrical, and optical characteristics have been examined using the GGA with PBE functional. It was found that pure CaO is more stable than with oxygen vacancies. DOS discloses direct relation between donor levels and oxygen vacancies. Oxygen vacancies have inverse effect on band gap, optical absorption coefficient and HOMO-LUMO energy states, with increasing oxygen vacancies band gap, optical absorption coefficient and HOMO-LUMO energy states decrease.

By J.F. Mammone et al.[53], following research has been carried out Lower-pressure data and an EOS estimated from shock-wave tests coincide with static higher-pressure data obtained from experiments on the EOS of the NaCl type and CsCl type phases of CaO in the range of 1 bar–650 kbar. The features of CaO may be acceptable to ideas of the formation of the earth through in-homogeneous acceleration since the density of the CsCl type phase is similar to that of the lower mantle. Calcium oxide (CaO) experiences a volume reduction of 11% following shock load in the range 0.6 and 0.7 Mbar. This gap is thought to be the result of a phase change from NaCl type to CsCl type structure.

By D.M. Hoat et al.[54],following research has been carried out It has been reported that the structure, electrical, optical, and thermoelectric characteristics of the CaO mono-layer and bi-layers with AA and AB stacking are examined using FP-LAPW approach and SCBTT (semi-classical Boltzmann transport theory).As long as they exhibit a broad absorption band and higher adsorption coefficient, CaO mono-layers and bi-layers seem to be promising materials for use in optoelectronic devices as ultraviolet detectors and absorb. According to simulations, incoming light that is in-plane polarized may be more effective at stimulating electronic transitions than light that is polarized perpendicularly. Lastly, the thermoelectric characteristics of the layers in question are computed and described. These characteristics include the Seebeck coefficient, electrical conductivity, electronic thermal conductivity, and power factor. According to research, the thermoelectric uses may benefit most from the AA-stacking. The results provided here could provide low-dimensional broad band gap materials with some useful theoretical direction.

Chapter 3

Calculation Methods

To evaluate the properties of any system, one needs to find the stable energy configuration of the system. This can be done by minimizing the energy of the system for a given configuration. The energy of a many-body system can be described through Schrodinger wave equation. However, the analytical solutions of Schrodinger wave equation for many-body systems are nearly impossible. Therefore, numerical methods such as Molecular Dynamics and Density Functional Theory (DFT) are developed and tested for solving such systems. Here we have used First-principle DFT calculations to determine the structural, optical and thermoelectric properties of our system[55].

3.1. Density Functional Theory

DFT is a strong technique for solving quantum mechanical systems, DFT has enormous significance for investigating a large number of properties in atoms, solids, or molecules. The quality of DFT as compared to other methods can be satisfied by the interaction of electrons or by transforming it into many-body systems. The computational buildup of DFT makes it user-friendly for every research related to the first-principle analysis of any material.

$$\left[\frac{-\hbar^2}{2m}\sum_i \nabla_i^2+\sum_i V_{ext}(r_i)+\frac{1}{2}\sum_{i\neq j}\frac{e^2}{(r_i-r_j)}-E\right]\psi(r_1,\ldots r_N)=0$$

The above equation depicts the energy contributions in terms of kinetic energy, and electron-electron interaction respectively, where sub-scripted r represents position of electrons, V_{ext} is external potential and following that the next term is the potential term. the energy equation cannot be solved exactly due to its complex nature and one needs to make

some approximations to make it simple and get an approximate solution way much closer to the exact solution. The approximations used in DFT approach are listed below.

3.1.1. Theorems of Hohenberg – Kohn

DFT approach considers every variable in terms of electron density function. This concept was at first introduced by Thomas and Fermi. Further, this concept was used by P. Hohenberg and W. Kohn and presented in the form of two theorems, which are of fundamental importance in DFT approach. Both the theorems are explained below[56].

3.1.1.1. First Theorem

When an external potential is applied to a particular system, in the ground state, the link between potential and particle density is direct. In other words, it's not possible for different values for the external potential to correspond to the same ground state energy.

3.1.1.2. Second Theorem

A widespread energy functional E[n] can be expressed as a function of n(r) density for any internal potential $V_{ext}(r)$. The system's ground state energy is the functional energy's minimum value for a given $V_{ext}(r)$. The system's genuine ground state density is the density with the lowest value. The above function can be displayed in the following format:
For a given external potential, $V_{ext}(r)$, an energy functional E[n] may be specified as a function of n(r) density. For a specific external potential, $V_{ext}(r)$ minimized value of functional energy corresponds to the ground state energy of the system. The density that has minimum energy corresponds to the actual ground-state density of the system $n_0(r)$. The functional can be written as

$$T[n(r)]+V^{ee}[n(r)]-\int V_{ext}(r)n(r)dr$$

So, the functional given above represents the ground-state energy of a particular system.

3.1.2. Kohn-Sham equations

As listed above theorems of P. Hohenberg and W. Kohn introduced the idea of electronic density, which slight simplified the problem of many-body system. In1965 Kohn and Sham presented the idea under the influence of an effective potential created by nuclei and other electrons, a significant number of interacting electrons are replaced with an equivalent non-interacting system[57]. Their idea was to use a non-interacting comparable technique to obtain the actual system's ground state parameters. As a result of this formalism, ground state energy is described as

$$E\rho \; = \; T_{s\rho} + \int v_{ext}(r)\rho(r)dr + + \frac{1}{2}\iint \frac{\rho(r)\rho(r)}{r_{1,2}} \; dr_1 dr_2 \; + E_{xc}[\rho]$$

The non-interacting electron contribution, nucleus potential, and Hartree-Fock potential are defined by the first four terms on the right-hand side of the equation. The last term is the unknown exchange-correlation potential.

The Kohn sham equation could not give the accurate results for exchange-correlation potential but provides the basis of DFT and needs various approaches for getting results very closer to actual ones. DFT is equipped with different accurate and successful approximations. However, the more general approximations are Local Density Approximation (LDA) and Generalized Gradient Approximation (GGA) which include PBE and PBEsol, mBJ, and TB-mBJ, and Hybrid functional which include HSEo6 , few of them are discussed below

3.1.3. Local density approximation (LDA)

LDA is one of the effortless approaches for computing the energy of exchange-correlation. Local spin density approximation (LSDA) is used for spin systems[58–61]. In the LDA exchange-correlation density is replaced locally with the K-H equation in estimated local density. LDA is

based on the approximation that electron density is not same on all points, so molecular solid density is considered by utilization of homogeneous electron gas[62,63]. LDA is very much helpful for structural properties, however, it has some limitations for systems having electrons located and correlated. The limitations to lessen above mentioned issues a lengthy range of gradient effects are integrated with the inclusion of gradient correction in LDA

3.1.4. Generalized gradient approximation (GGA)

In some cases, the result of approximating local density calculations does not match experimental data, so a homogenous gas of electrons with gradient correction is used. The gradient can be a function of spin density and gradient as well. Electronic gradient density and uniform density affect the approximation of local density. This new approach is called as GGA, and it is more precise than LDA.

GGA modifies physical attributes such as bond length, energy at ground state, molecules, solids, and their band structures at the ground state. GGA is more effective and exact as compared to the LDA approximation[64–66]. Further research has revealed that the computation of exchange-correlation electricity has a 1% error rate, whereas LDA has a 14 percent error rate, indicating that GGA is the optimal approach for many-body systems. However, when compared to practical and computational results, these approximations are fairly restrictive, bandgap calculations are inadequate, and they do not yield remarkable results for thermoelectric and optical characteristics. Perdew and a coworker came up with a new notion for a straightforward solution, however it doesn't meet DFT's requirements.

The theory proposed by Handy and coworkers is not supported by this technique. Xu and Goddard gave XPBE a new practical makeover. This method is useful for identifying a wide range of features. Cohen and Wu developed a new term to boost the F_{xc}(enhancement factor) factor and improve outcomes, which works in a positive way. Xu and Goddard presented XPBEGGA, a new functional, it is of great use for many properties. Cohen and Wu enlightened with a new technique to increase the F_{xc} factor for better results, it works fine.

Kohn sham (KS) equations are solved for KS orbitals as in an expanded scheme for solids, but the wave function corresponds to every non interacting electron extendable across the whole solid. Bloch's theorem is given for this problem as

$$\Psi_{nk}(r)=e^{(ik.r)}u_{nk}(r)$$

This expression shows the correspondence of plane wave and lattice periodicity. The wave function is based on the plane wave, and it makes a fine choice for basis sets.

3.1.5. Trans and Blaha modified Becke-Johnson exchange correlation functional (TB-mBJ)

GGA and Trans Blaha modified Backe Johnson (TB-mBJ) potential are both taken into account as correlation exchange, where TB-mBJ ,is applied on GGA because GGA underestimates band gap[67,68]. The improved band gap is obtained using mBJ, which is far better than GGA and way much closer to experimental results. In order to resolve issues related to bandgap Tran and Blaha examined the exchange potential of Becke Johnson (BJ), which has given the optimized exchange potential. BJ potential provides good outcomes than LDA and GGA, but it also underrates band gap outcomes[69,70]. Trans and Blaha (TB) modified the BJ and which is familiar with the name periodic TB-mBJ or mBJ potential. It gives improved band gap results, which are comparable to experimental results.

3.2. Computational Details

All calculations were carried out using first principles calculations according to Full potential linearized augmented plane waves (FP-LAPW), incorporated in the WIEN2k[71–75] package the BoltzTraP code. PBE-GGA correlation functional was incorporated initially which underestimated the band gap. To address the issue TB-mBJ was applied onto PBE-GGA. $R_{MT}K_{max}$ (smallest atom radius muffin tin multiplied by largest k vector) was chosen 7 for all systems. Charge convergence was set to 10^{-5} Ry. K mesh for SCF calculation was taken as$10 \times 10 \times 10$, each for pure and 25% with oxygen vacancies and doped, while for 3.12% O vacancy, it was

chosen as $7 \times 7 \times 7$. Denser K mesh for optical, electronic and thermoelectric properties for all systems was chosen $21 \times 21 \times 21$.

Chapter 4

Results and analysis

4.1. Structural Properties

the lattice constants for all the doped and undoped systems are given below.

Table 4.1:List of lattice constants for all systems

Compound	Lattice constants
CaO	4.84
CaO 25% Zn doped	4.73
CaO 25% Cd doped	4.80
CaO 25% O vacancy	4.84
CaO 3.12% O vacancy (2*2*2)	9.68

4.1.1. Calcium Oxide

Calcium Oxide (CaO) has face centered cubic structure, in which calcium atoms occupying positions of all six faces and on each corner and remaining positions are occupied by oxygen atoms[54]. Following is given figure of structure and volume vs Energy, the structure with minimum energy was used as input to compute other quantities

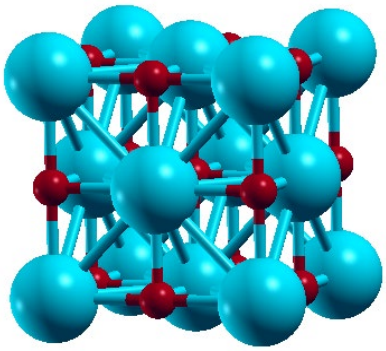

Figure 4.0.1: CaO crystal structure

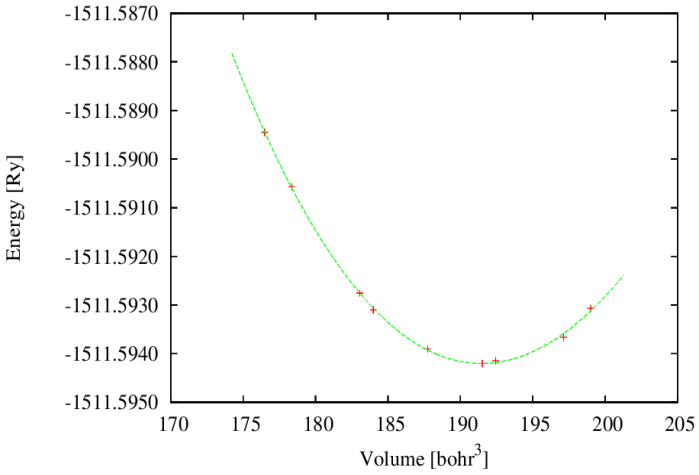

Figure 4.0.2: Volume optimization of CaO

4.1.2. Calcium Oxide 25% Cadmium doped

Here substitution doping was performed by replacing one calcium atom out of four with a cadmium atom, as we can see after doping corner calcium atoms are replaced by cadmium atoms, here are given the volume vs energy graph and the structure of calcium oxide doped with cadmium.

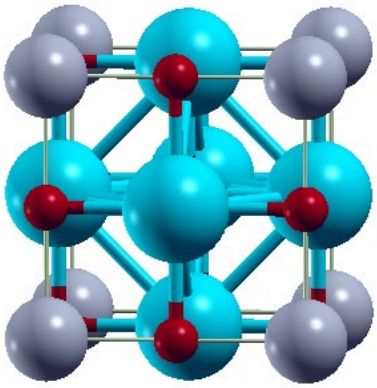

Figure 4.0.3: CaO 25% Cd doped crystal structure

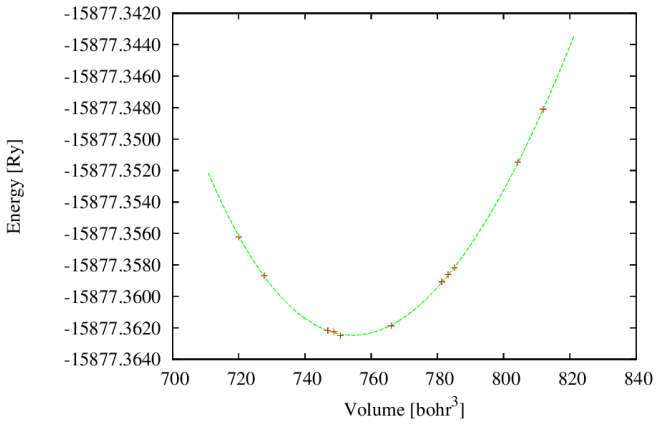

Figure 4.0.4: Volume optimization of CaO 25% Cd doped

4.1.3. Calcium Oxide 25% Zinc doped

Here substitution doping was performed by replacing one calcium atom out of four with zinc atom, here as we can see after doping corner calcium atoms are replaced by zinc atoms, here are given the volume vs energy graph and the structure of calcium oxide doped with zinc.

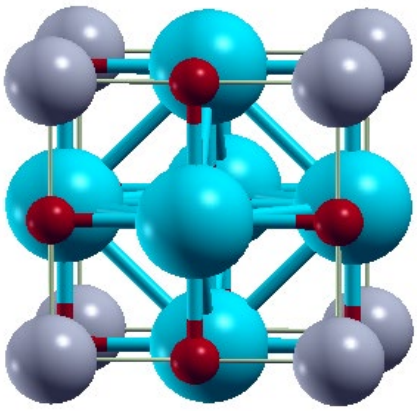

Figure 4.0.5: CaO 25% Zn doped crystal structure

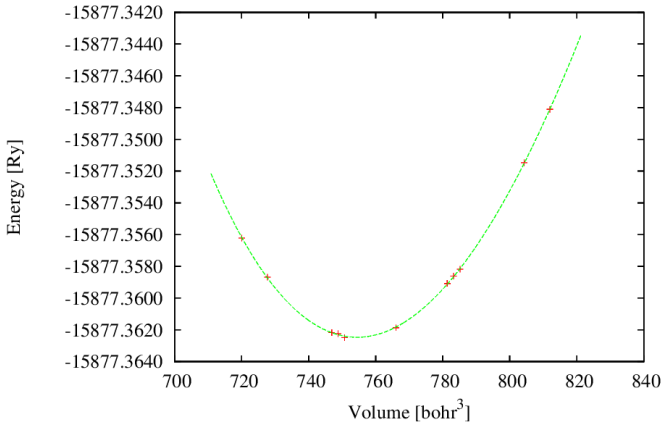

Figure 4.0.6: Volume optimization CaO 25% Zn doped

4.1.4. Calcium Oxide with Oxygen vacancies

For creating 25% Oxygen vacancy one oxygen atom was removed out of four oxygen atoms. For creation of 3.12% Oxygen vacancy, the supercell of 2×2×2 was created whichgenerated 64 atoms in total, out of 32 Oxygen atoms one was removed to get the desired oxygen vacancy.

Following is given figure of supercell of Calcium Oxide.

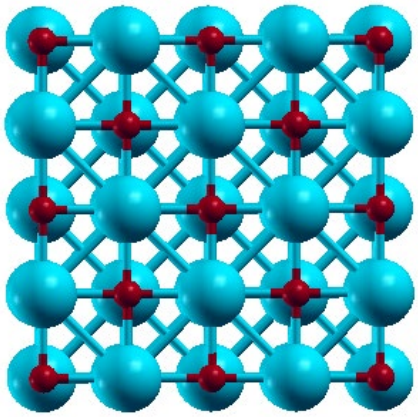

Figure 4.7: CaO supercell (2× 2 ×2) crystal structure

4.2. Electronic properties

4.2.1. Band Structure Analysis

Following are given results of band gap for all systems

Table 4.2:Band gap of all systems

Compound	E_g**(eV)**	
	PBE-GGA	**TB-MBJ on PBE-GGA**
CaO	3.68[54]	6.00
CaO 25% Cd doped	1.41	4.25
CaO 25% Zn doped	1.31	4.47
CaO 25% O vacancy	0	1.51
CaO 3.12% O vacancy	0.87	3.19

4.2.1.1. Calcium Oxide

CaO as reported experimentally has direct band gap of 7.1 eV[49]. We have found its band gap using PBE-GGA gamma to X indirect band 3.67[52], which is clearly underestimated, so TB-mBJ was incorporated to get the value closer to experimental, so it was improved to 6 eV indirect gamma to X, and direct band gap is found from gamma to gamma around 7.4 eV which is closer to experimental band gap.

Following is shown band structure for CaO using PBE-GGA and TB-mBJ

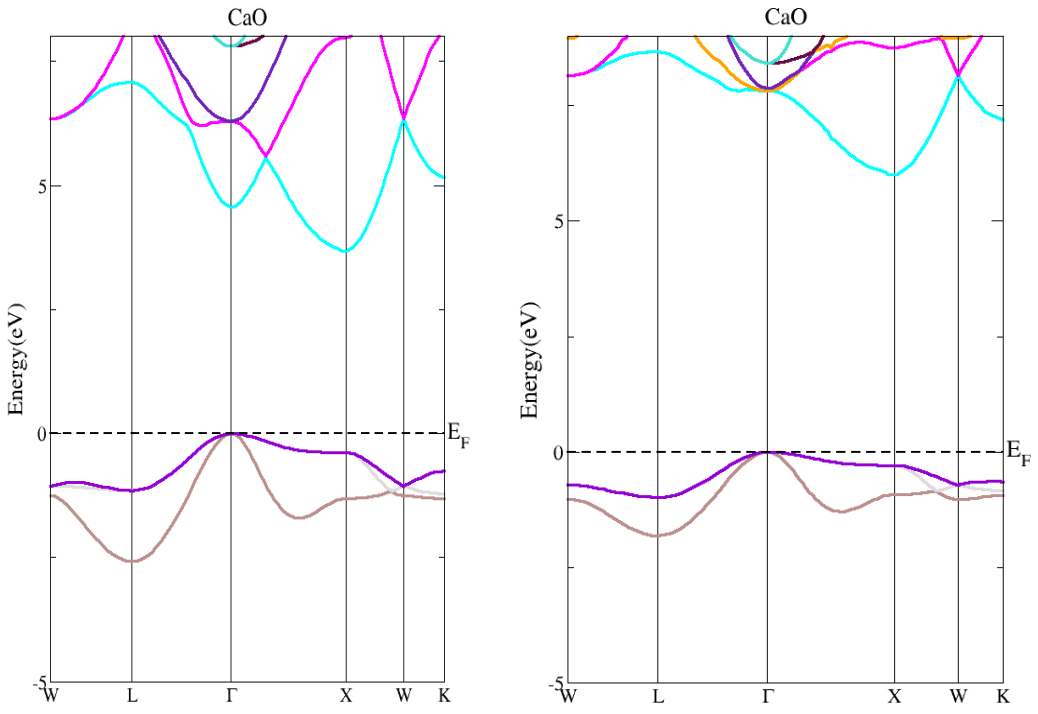

Figure 4.8: Band structure of CaO using: PBE-GGA (left) and TB-mBJ (right)

4.2.1.2. Doped Calcium Oxide

Below is shown band structure of Calcium oxide 25% doped each with cadmium and zinc doping has clearly shown decrease in band gap, as pure calcium oxide was found to have 6.0 eV band gap and when doped with cadmium it has resulted in 4.25 eV band gap, and while doping the same percentage with zinc has given band gap 4.47eV. We will further discuss contributions of different atoms in the density of states section.

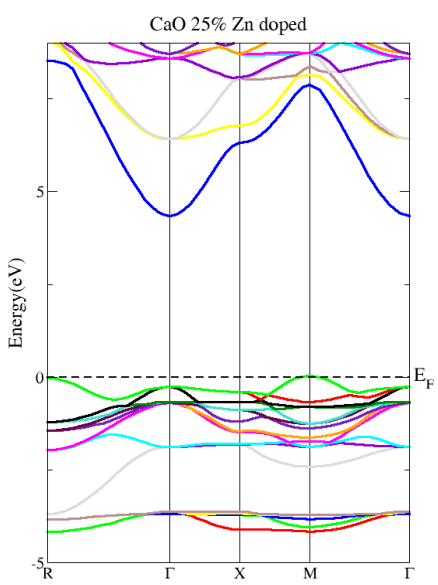

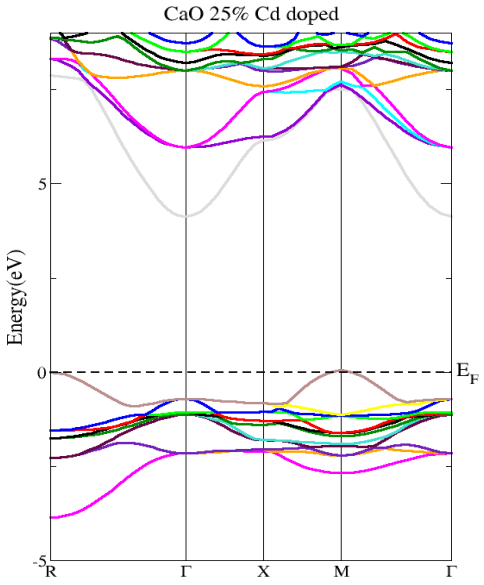

Figure 4.9: Band structure of CaO 25% Zn doped *Figure 4.10: Band structure of CaO 25% Cd doped*

4.2.1.3. Calcium Oxide with Oxygen vacancies

Creating oxygen vacancies reduces the band gap further, it has reduced band gap more than doping with zinc or cadmium. Oxygen vacancies have direct relation with the decrease in the band gap, as the vacancies increase band gap decreases, band gap with 3.12% oxygen vacancy is given as 3.19 eV and it is further reduced to 1.51 eV when oxygen vacancies increased to 25%.We will further discuss the contributions of individual atoms and formation of donor levels in the section of density of states.

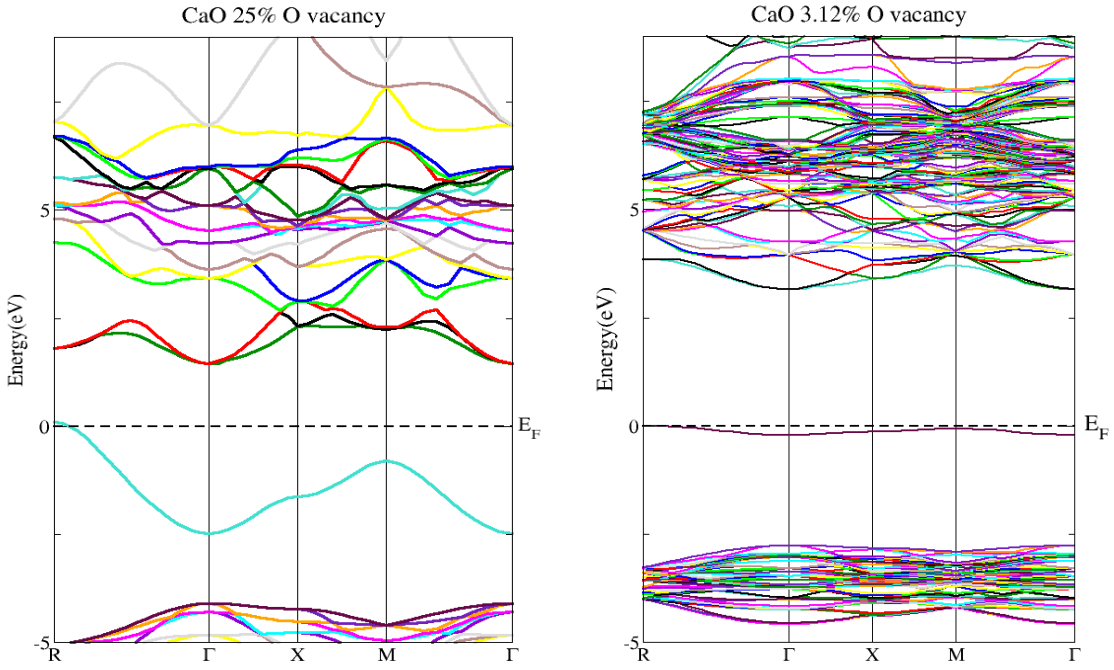

Figure 4.0.11: Band structure of CaO with 25% Oxygen vacancy(left) CaO with 3.12% O vacancy(right)

4.2.2. Density of states

Following are given density of states for all systems

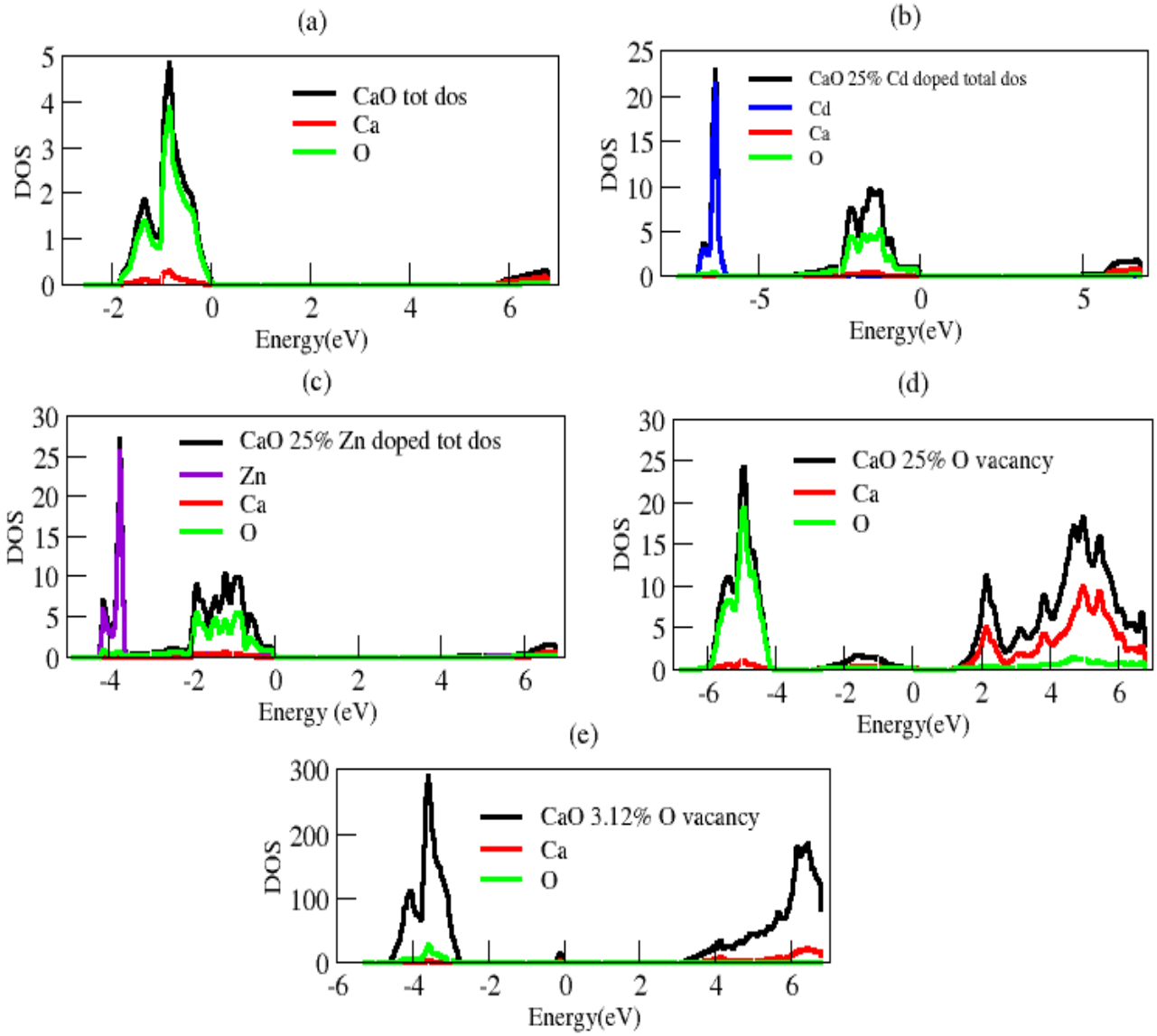

Figure 4.12: Density of states for all systems

4.2.2.1. Density of states of CaO

As we can see from the figure that dominant states are of oxygen atom in valence band and further it is noted that calcium atom has very little contribution in the states lower than valence

band and in valence band, but it is dominant in the conduction band where oxygen contribution is very less in conduction band.

5.2.2.2. Calcium oxide 25% doped with cadmium

As shown in the figure cadmium dominates in the states lower than the valence band, and has very little contribution in valence band and no contribution in conduction band, oxygen is much dominant valence band and has very less contribution in conduction band. Calcium has more contribution in valence band then cadmium atom and less than oxygen atom, and in conduction band calcium has more dominance than both other.

4.2.2.3. Calcium oxide 25% doped with zinc

As shown in the figure c, zinc dominates in the states lower than the valence band, and has very little contribution in valence band and no contribution in conduction band, oxygen is much dominant in valence band and has very less contribution in conduction band. Calcium has more contribution in valence band then cadmium atom and less than oxygen atom, and in conduction band calcium has more dominance than both other. Further it can be seen that the trend followed in zinc and cadmium is very much similar.

4.2.2.4. Calcium oxide with 25% oxygen vacancy

As seen in figure d, the oxygen atom has dominant contribution only in states lower than valence and has very less contribution in valence band and a little contribution in conduction band whereas calcium has little contribution in valence band, but higher than oxygen and has dominant contribution in conduction band. The enormous contribution of calcium atom is because of oxygen vacancy as oxygen atom is removed so its states have decreased and calcium dominates.

4.2.2.5. Calcium oxide with 3.12% oxygen vacancy

As depicted in the figure e, oxygen atom dominates in the states lower than and has very less contribution in valence band and very less, no any considerable contribution in conduction band whereas calcium atom dominates in the conduction band and has less contribution in valence band and reasons are same as mentioned above in explanation of figure d.

4.3. Thermoelectric properties

Calcium oxide and calcium hydro oxide are used for thermal storage, our main aim in this theses are to use them as Thermoelectric and optoelectronic devices, first of all we are checking effect of doping and oxygen vacancies on thermoelectric properties.

Following are discussed thermoelectric properties in detail

4.3.1. Thermal conductivity (electronic contribution)

Thermoelectric materials having the least thermal conductivity are having the higher figure merit hence the efficiency as discussed earlier, here it can be seen that the systems with oxygen vacancies have lower thermal conductivity than doped and pure, doped calcium oxide is having

more thermal conductivity than the pure. Let's first discuss all properties individually and we will sum up in conclusion. Following is shown thermal conductivity graph.

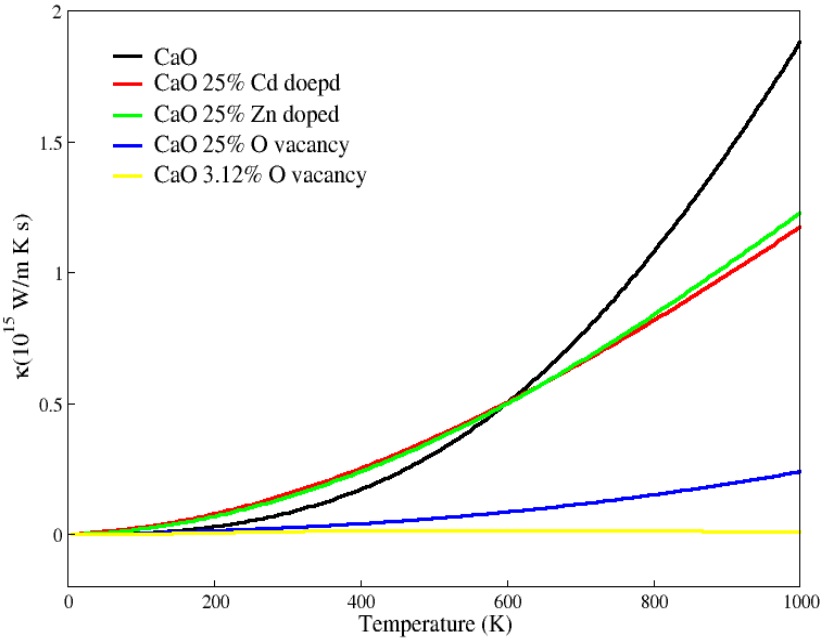

Figure 4.0.13: Temperature vs thermal conductivity graph

4.3.2. Electrical conductivity

Thermoelectric materials are considered the best having large electrical conductivity as discussed earlier ,here as we can see that doped materials are having higher electrical conductivity than pure and with oxygen vacancies, of which cadmium doped has higher value than zinc doped, whereas oxygen vacancies have the least value of electrical conductivity for all temperatures ,of which with 25% oxygen vacancy is having higher value than with 3.12% oxygen vacancy .pure

calcium oxide has lower value than doped and higher than with oxygen vacancy. Following is given temperature vs electrical conductivity graph.

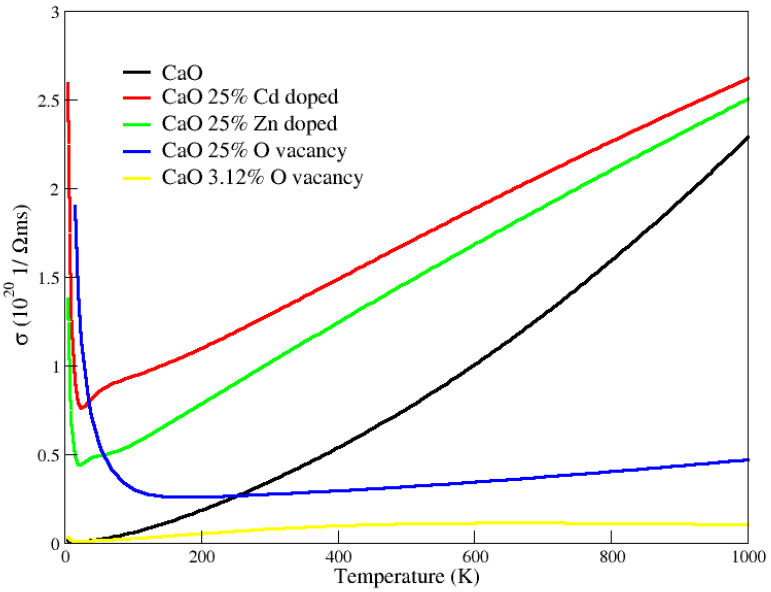

Figure 4.0.14: Temperature vs electrical conductivity graph

4.3.3. Seebeck Coefficient

Thermoelectric materials are having higher efficiency which have higher value of Seebeck coefficient as discussed earlier, here highest value for Seebeck coefficient is of pure calcium oxide and then there is dominance of 3.12% oxygen vacancy till around 400 K and then it has decreasing trend and ends at least value from 600 K to 1000K ,after that zinc doped calcium oxide has higher value for all temperatures then there is dominance of cadmium doped and at the end the least value till 600 K is possessed by 25% oxygen vacancy and has value greater than 3.12% oxygen doped from 600 K onwards .Therefore pure material has the best Seebeck coefficient.

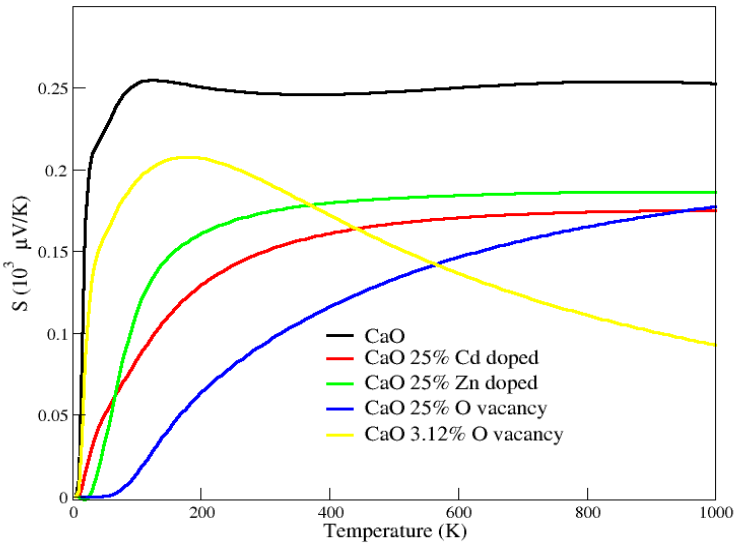

Figure 4.0.15: Temperature vs seebeck coefficient graph

4.3.4. Electronic Power Factor

Thermoelectric materials are efficient converter of heat into electricity ,which have higher value of electronic power factor ,here as shown in the figure below the higher electronic power factor value is of doped calcium oxide till around 500 K, as we are mostly interested in the temperatures around room temperature ,the materials which are efficient at the room temperature can widely be used in home appliances, after doped pure calcium oxide has the greater value than calcium oxide with oxygen vacancies till around 500 K, and for temperatures more than 500 K it is dominant of all. Calcium oxide with oxygen vacancies have least value as compared to doped and pure. In oxygen vacancies with 25% oxygen vacancy is more dominant values than with 3.12% oxygen vacancy.

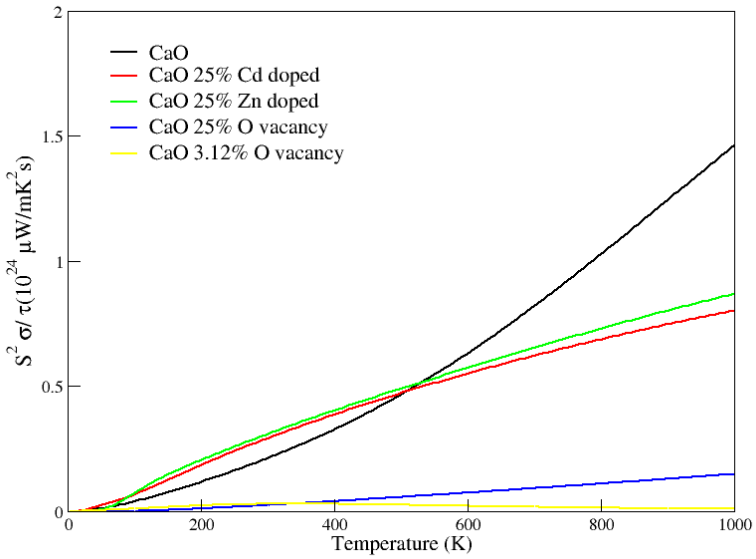

Figure 4.16: Temperature vs electronic power factor graph

4.3.5. Thermoelectric figure of merit

Thermoelectric figure of merit is the measure of efficiency of thermoelectric materials, the higher the value of figure of merit the better the performance of thermoelectric materials. As we can see from the figure given below, we have got fruitful results for creating oxygen vacancy, the value of calcium oxide with 3.12% oxygen vacancy dominates from 300 K to 1000 K which shows with oxygen vacancy it can be potential thermoelectric material, pure calcium oxide has less value than 3.12% oxygen vacancy and greater than doped and with 25% oxygen vacancy ,after pure calcium oxide zinc is third best performing material after that on number four comes the cadmium

oxide and least is for calcium oxide with 25% oxygen vacancy .Following is given graph of temperature vs figure of merit.

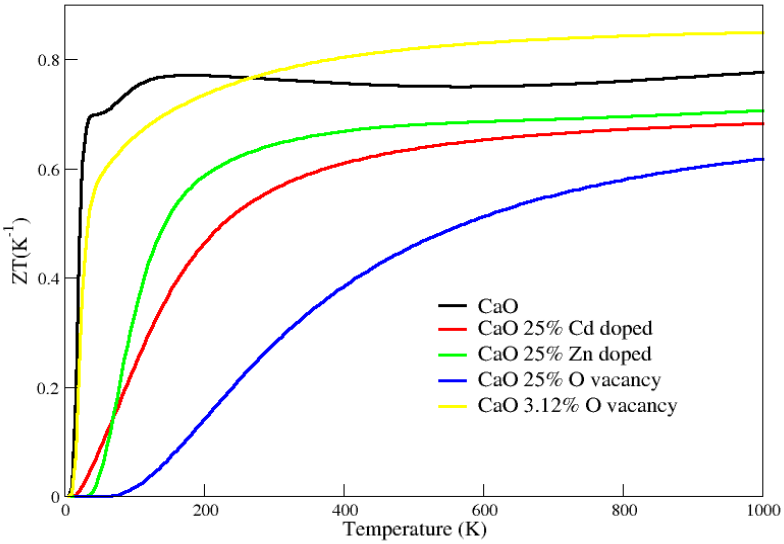

Figure 4.17: Temperature vs ZT graph

4.4. Optical properties

As discussed in electronic properties section there has been considerable effect on band structures of calcium oxide doped with cadmium and zinc and with oxygen vacancies, as semiconductors are considered good for solar cell fabrication and other optoelectronic devices.

Following are discussed optical properties

4.4.1. Absorption coefficient

The materials having higher absorption in the visible region are considered good for solar cell fabrication as discussed earlier, visible range is till 3 eV, as we can see in that domain there is dominance of calcium oxide with 25% oxygen vacancy after that there starts the absorption of 3.12% oxygen vacancy then absorption starts for doped with zinc and cadmium and at the last around 6.0 eV starts the absorption of pure calcium oxide. Here it is very clear that absorption

results of calcium oxide doped and with oxygen vacancies has improved and specially with oxygen vacancies it can be a potential solar cell fabrication material. Following is given the incident photon energy vs absorption coefficient.

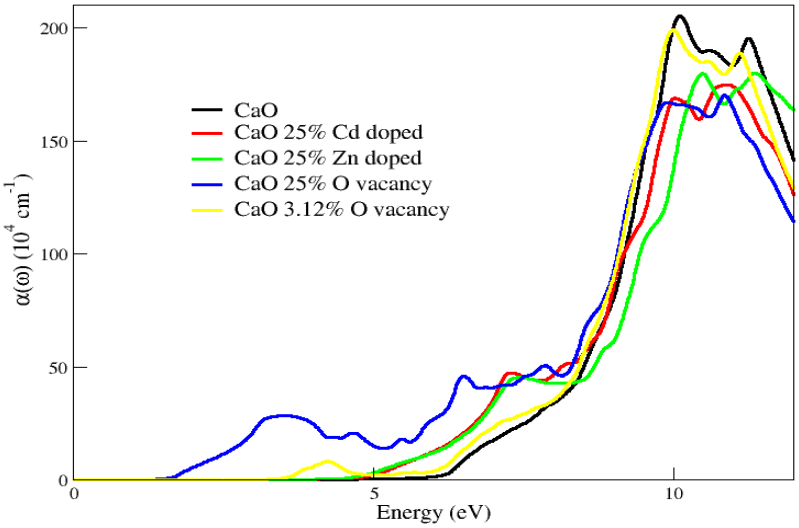

Figure 4.18: Energy vs absorption coefficient graph

4.4.2. Refractive index

High refractive record materials are logically predominant in optoelectronics. Their principal use is for upgrading the visual properties of electronic showcases, which incorporates LCDs, OLEDs, and quantum spot (QDLED) TVs66.

Here we ca see that dominance is of 25% oxygen doped calcium oxide till around 4 eV of incident photon energy and then there is dominance oxygen vacancy 3.12% and 25 doped with cadmium and zinc, all have overlapping values till around 4 evilest value in the given range is of pure

calcium oxide, so the doped and with oxygen vacancies can be considered potential materials for various optoelectronic devices as discussed above.

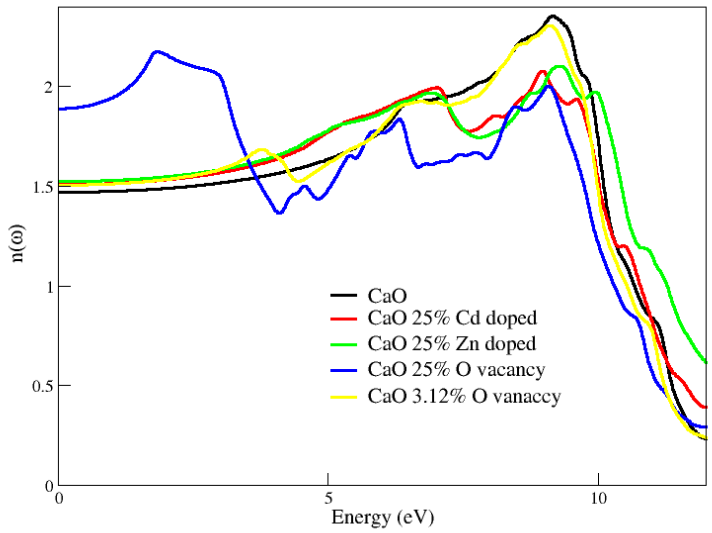

Figure 4.19: Energy vs refractive index graph

4.4.3. Extinction coefficient

'As 'extinction coefficient (k)' is a measure of light lost due to scattering and absorption per unit volume98,here we can see that extinction coefficient for 25% oxygen vacancy has the highest value till around 7 eV and 3.12% oxygen vacant has the second highest value from 3 eV to 5eV ,from 5eV to around 7 eV doped with cadmium and zinc has the joint second highest value after

the 25% oxygen vacant, in the region described here pure calcium oxide has the least value. Following is given energy of incident photon vs extinction coefficient graph.

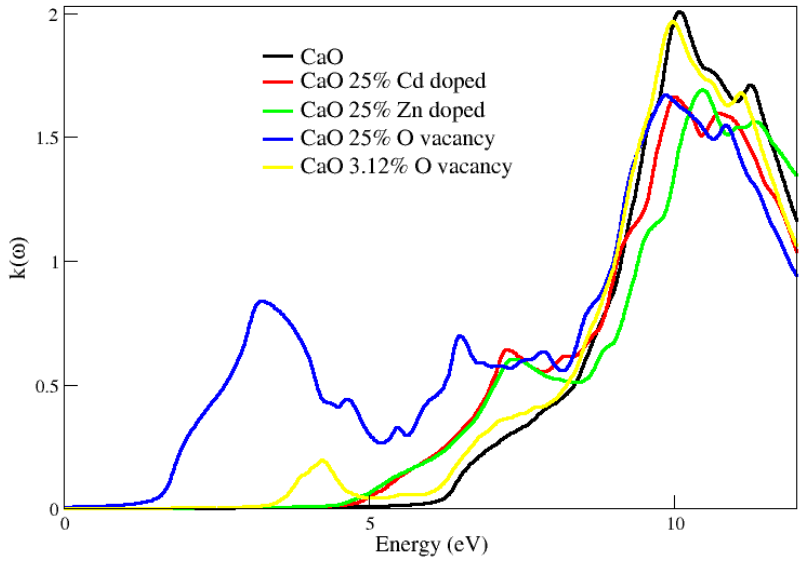

Figure 4.20: Energy vs extinction Coefficient graph

4.4.4. Reflectivity

Reflectivity is the measure of bouncing back of light from a surface, it is used where we do not want light to penetrate in any surface rather want light to bounce back. Here as we can see in the graph calcium oxide with 25% oxygen vacancy has the highest value till around 4 eV, all materials are having almost overlapping values after that with minimal differences. Following is shown energy of incident photon vs reflectivity graph.

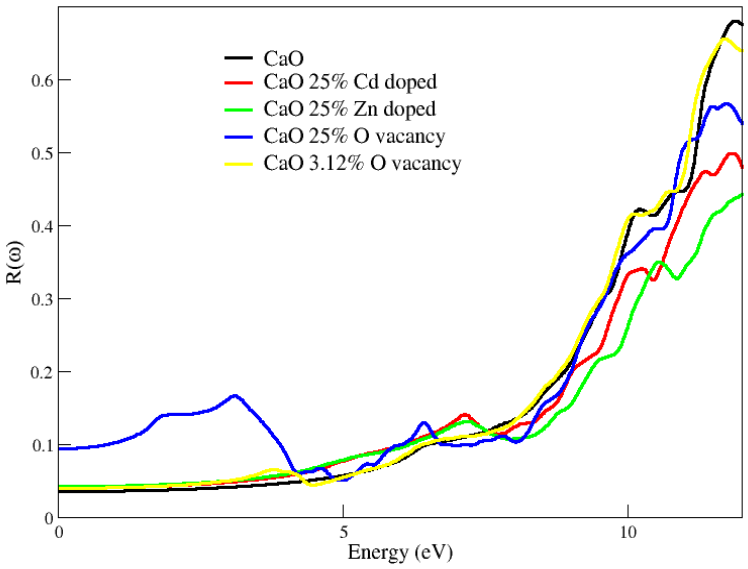

Figure 4.21: Energy vs reflectivity graph

4.4.5. Optical conductivity

Optical conductivity starts for calcium oxide with 25% oxygen vacancy from 1.5 eV has highest value till around 7 eV, from 3 eV to 5 eV calcium oxide with 3.12% oxygen vacancy dominates, from 5 eV onwards doped with cadmium and zinc has the joint second highest values after 25% oxygen vacant till 7 eV dominate all from 7 eV to 7.5 eV .The peak value of optical

conductivity for pure calcium oxide occurs at 10 eV, which is the largest of all at this energy of incident photon.

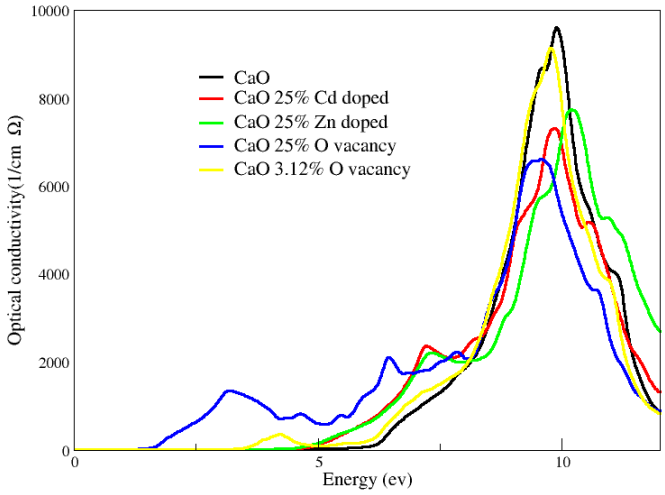

Figure 4.22: Energy vs optical conductivity graph

4.4.6. Optical loss

To discuss the trend of the optical loss ,as shown in the graph below as the energy of incident light increases ,optical loss increases ,the calcium oxide with 25% oxygen vacancy starts at the earliest energy of around 1 eV and dominates all the way having peak around 3.5 eV,then notable contribution is from 3.12% oxygen vacancy from 2.5 eV to 5 eV with peak around 5eV

,from 5 eV on wards doped with cadmium and zinc have the second largest value all along, the least value is for pure calcium oxide all along.

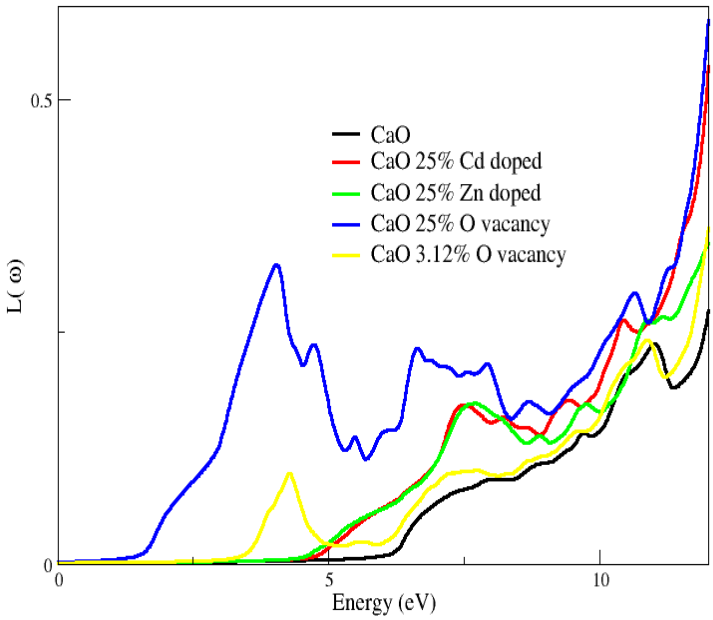

Figure 4.23: Energy vs elsoss function

4.4.7. Real part of dielectric function

Real part is derived from imaginary part and is used in finding various optical properties as discussed earlier. The real part is dominated by 25% oxygen doped from 0 to around 2.5 eV, after that it's value shoots down and has the least value of all till 10 eV. Second highest value from the start to around 7 eV is of doped calcium oxide with cadmium and zinc and pure calcium oxide has much similar trends to doped materials.

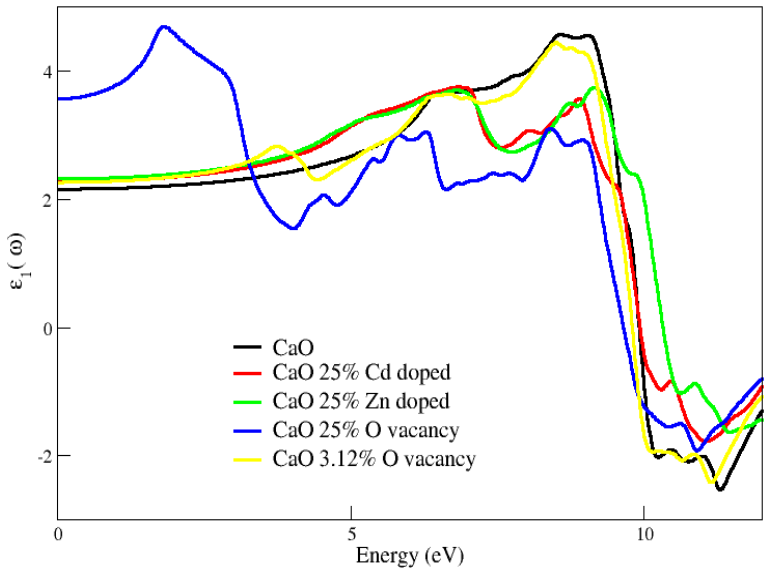

*Figure 4.24: Energy vs real part of dielectric function****5.4.8. Imaginary part of dielectric function***

Imaginary part of dielectric function is used to calculate real part of dielectric function and some other optical properties. As shown in the graph below 25% oxygen doped calcium oxide has the higher value of all from starting to 8 eV and it has decreasing trend from and attains the -2 value at around 11 eV, whereas calcium oxide doped with cadmium and zinc and pure calcium oxide are having almost similar trends as can be seen in the graph. Following is shown the graph of energy vs imaginary part of dielectric function.

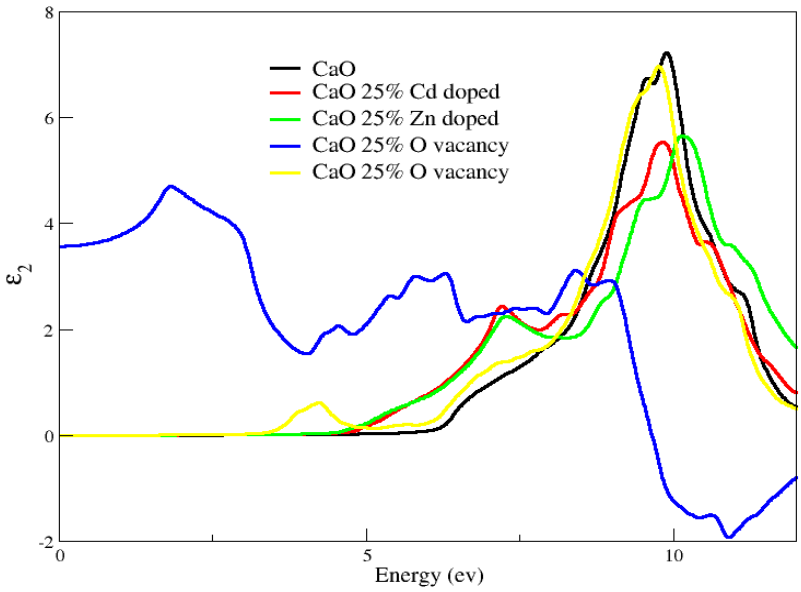

Figure 4.25: Energy vs imaginary part of dielectric function

Chapter 5

Conclusion

In this work, we have used density functional theory to investigate the electronic, optical, and thermoelectric properties of pure CaO, metal doped, and with oxygen vacancies. CaO with Oxygen vacancies was found to have more influence on bandgap than doped with zinc and cadmium. Optical absorption in the visible region was also dominated by CaO with oxygen vacancies. In the thermoelectric studies, we found out a large value for electronic conductivity for doped CaO and the value for thermal conductivity at all temperatures was the least for CaO with oxygen vacancies, and the ZT value was highest for 3.12% oxygen vacant CaO. From thermoelectric results, it can be concluded that improved results with better control on bandgap can be achieved if the material is doped together with oxygen vacancies creation.

Future directions

The current stage of this work opens many directions for further modifications. As discussed earlier in thermoelectric properties, CaO doped with metals and having oxygen vacancies has the highest values of electronic conductivity and least values of thermal conductivity which suggests CaO co-doped with oxygen vacancies can be a potential thermoelectric material. Here we have only worked for bulk CaO pure and doped, further, we can shift to 2d structure to get better results for pure and doped cases, as in 2D band gap is reduced due to grain boundaries, which can help us make our material semiconductor not only with oxygen vacancies but also with doping, as semiconductors are considered best thermoelectric and optoelectronic materials. So 2D CaO structure doped and having oxygen vacancies can be a potential thermoelectric and optoelectronic material.

References

1. Hatfield JL, Sauer TJ, Prueger JH. Managing soils to achieve greater water use efficiency: A review. *Agronomy Journal*. 2001;93(2):271-280. doi:10.2134/AGRONJ2001.932271X
2. Santanello JA, Dirmeyer PA, Ferguson CR, et al. Land–Atmosphere Interactions: The LoCo Perspective. *Bull Am Meteorol Soc*. 2018;99(6):1253-1272. doi:10.1175/BAMS-D-17-0001.1
3. Wright GC, Rao RCN. Groundnut water relations. *The Groundnut Crop*. Published online 1994:281-335. doi:10.1007/978-94-011-0733-4_9
4. Kaufman YJ, Tanré D, Dubovik O, Karnieli A, Remer LA. Absorption of sunlight by dust as inferred from satellite and ground-based remote sensing. *Geophysical Research Letters*. 2001;28(8):1479-1482. doi:10.1029/2000GL012647
5. Davies PA. Sustainable energy systems for seawater reverse osmosis desalination. *Emerging Membrane Technology for Sustainable Water Treatment*. Published online March 18, 2016:111-134. doi:10.1016/B978-0-444-63312-5.00005-X
6. Hesaraki A. Low-Temperature Heating and Ventilation for Sustainability in Energy-Efficient Buildings.
7. Jouhara H, Energy AO, 2018 undefined. Industrial waste heat recovery. *Elsevier*. https://www.sciencedirect.com/science/article/pii/S0360544218313070
8. Luo A, Fang H, Xia J, Resources BL, Recycling C and, 2017 undefined. Mapping potentials of low-grade industrial waste heat in Northern China. *Elsevier*. https://www.sciencedirect.com/science/article/pii/S0921344917301726
9. Loni R, Najafi G, Bellos E, Rajaee F, … ZSJ of cleaner, 2021 undefined. A review of industrial waste heat recovery system for power generation with Organic Rankine Cycle: Recent challenges and future outlook. *Elsevier*. https://www.sciencedirect.com/science/article/pii/S0959652620351143
10. Zeb K, Ali SM, Khan B, et al. A survey on waste heat recovery: Electric power generation and potential prospects within Pakistan. *Renewable and Sustainable Energy Reviews*. 2017; 75:1142-1155. doi: 10.1016/ J. RSER.2016.11.096

11. Saeed Y. Tuning the Transport Properties of Layered Materials for Thermoelectric Applications using First-Principles Calculations. Published online 2014.
12. Thermoelectric Effect – Yasin ÇAPAR. https://yasincapar.com/thermoelectric-effect/
13. Beretta D, Neophytou N, Hodges JM, et al. Thermoelectrics: From history, a window to the future. *Materials Science and Engineering R: Reports*. 2019;138. doi: 10.1016/J.MSER.2018.09.001
14. Riffat S, engineering XMA thermal, 2003 undefined. Thermoelectrics: a review of present and potential applications. *Elsevier*. https://www.sciencedirect.com/science/article/pii/S1359431103000127
15. Riffat SB, Ma X. Thermoelectrics: A review of present and potential applications. *Applied Thermal Engineering*. 2003;23(8):913-935. doi:10.1016/S1359-4311(03)00012-7
16. Bell LE. Cooling, Heating, Generating Power, and Recovering Waste Heat with Thermoelectric Systems. *Science (1979)*. 2008;321(5895):1457-1461. doi:10.1126/SCIENCE.1158899
17. Shi X, Zhang W, Chen LD, Yang J. Filling fraction limit for intrinsic voids in crystals: Doping in skutterudites. *Physical Review Letters*. 2005;95(18):185503. doi:10.1103/PHYSREVLETT.95.185503/FIGURES/4/MEDIUM
18. Dirl R, Weinberger P. Group Theory in Materials Science, Applications. *Encyclopedia of Condensed Matter Physics*. Published online January 1, 2005:290-302. doi:10.1016/B0-12-369401-9/01166-9
19. Martínez-Duart JM, Martín-Palma RJ, Agulló-Rueda F. Survey of Solid State Physics. *Nanotechnology for Microelectronics and Optoelectronics*. Published online 2006:21-53. doi:10.1016/B978-008044553-3/50005-9
20. Glazer AM. The reciprocal lattice. *A Journey into Reciprocal Space (Second Edition)*. Published online July 2021. doi:10.1088/978-0-7503-3875-2CH2
21. Misra PK. Basic Properties of Crystals. *Physics of Condensed Matter*. Published online 2012:1-35. doi:10.1016/B978-0-12-384954-0.00001-3

22. Papaconstantopoulos DA, Mehl MJ. Tight-Binding Method in Electronic Structure. *Encyclopedia of Condensed Matter Physics*. Published online January 1, 2005:194-206. doi:10.1016/B0-12-369401-9/00452-6
23. Itoh T, Araki T, Ashida M, Iwata T, Muro K, Yamada N. Optical Properties. *Springer Handbook of Materials Measurement Methods*. Published online 2006:531-607. doi:10.1007/978-3-540-30300-8_11
24. Gangwar P, Singh S, Khare N. Study of optical properties of graphene oxide and its derivatives using spectroscopic ellipsometry. *Applied Physics A: Materials Science and Processing*. 2018;124(9):1-8. doi:10.1007/S00339-018-1999-1/FIGURES/5
25. Saleem M, Atiq S, Ramay SM, et al. Investigations on electronic and optical properties of Ag: MoS2 co-sputtered thin films. *Chemical Physics Letters*. 2020;760:138032. doi:10.1016/ J. CPLETT.2020.138032
26. Grosso G, Parravicini GP. Optical Properties of Semiconductors and Insulators. *Solid State Physics*. Published online 2014:529-576. doi:10.1016/B978-0-12-385030-0.00012-8
27. Kanemitsu Y. Light Emission from Silicon Nanoparticles and Related Materials. *Comprehensive Semiconductor Science and Technology*. 2011;1-6:196-212. doi:10.1016/B978-0-44-453153-7.00075-4
28. Kanemitsu Y. Light Emission from Silicon Nanoparticles and Related Materials. *Comprehensive Semiconductor Science and Technology*. 2011;1-6:196-212. doi:10.1016/B978-0-44-453153-7.00075-4
29. Pierson J, Duverger E, Chemistry OBJ of SS, 2007 undefined. Experimental and theoretical contributions to the determination of optical properties of synthetic paramelaconite. *Elsevier*. https://www.sciencedirect.com/science/article/pii/S0022459607000047
30. Maghraoui-Meherzi H, Nasr T, in MDM science, 2013 undefined. Synthesis, structure and optical properties of Sb2Se3. *Elsevier*. https://www.sciencedirect.com/science/article/pii/S136980011200073X
31. Physics GRAJ of, 1970 undefined. A derivation of the macroscopic Maxwell equations. *aapt.scitation.org*. 1970;38(10):1842. doi:10.1119/1.1976000

32. Lax M, Nelson DF. Maxwell equations in material form. *Physical Review B*. 1976;13(4):1777-1784. doi:10.1103/PHYSREVB.13.1777
33. Xiong F, Wang YY, Chang RPH. Complex dielectric function of amorphous diamond films deposited by pulsed-excimer-laser ablation of graphite. *Physical Review B*. 1993;48(11):8016-8023. doi:10.1103/PHYSREVB.48.8016
34. Yang HU, Archangel JD', Sundheimer ML, Tucker E, Boreman GD, Raschke MB. Optical dielectric function of silver. *APS*. 2015;91(23):235137. doi:10.1103/PhysRevB.91.235137
35. Tanguy C. Analytical expression of the complex dielectric function for the hulthén potential. *Physical Review B - Condensed Matter and Materials Physics*. 1999;60(15):10660-10663. doi:10.1103/PHYSREVB.60.10660
36. Chiu M, Lee J, optics DSA, 1999 undefined. Complex refractive-index measurement based on Fresnel's equations and the uses of heterodyne interferometry. *opg.optica.org*. Accessed August 4, 2022. https://opg.optica.org/abstract.cfm?uri=ao-38-19-4047
37. Sokolik I, Andronova A, A TJAEnvironmentP, 1993 undefined. Complex refractive index of atmospheric dust aerosols. *Elsevier*. https://www.sciencedirect.com/science/article/pii/096016869390021P
38. Acevedo-Barrera A, García-Valenzuela A, Vázquez-Estrada O. Optical reflectivity of an interface with random refractive-index-contrast patterns. *Applied Optics, Vol 59, Issue 13, pp D221-D229*. 2020;59(13): D221-D229. doi:10.1364/AO.383166
39. Sun J, Lucyszyn S. Extracting Complex Dielectric Properties from Reflection-Transmission Mode Spectroscopy. doi:10.1109/ACCESS.2018.2797698
40. Pawade VB, Dhoble SJ, Swart HC. Graphene-based semiconductor nanocrystals for optoelectronics devices. *Nanoscale Compound Semiconductors and their Optoelectronics Applications*. Published online 2022:383-406. doi:10.1016/B978-0-12-824062-5.00010-5
41. Gu L, Srot V, Sigle W, et al. Band-gap measurements of direct and indirect semiconductors using monochromated electrons. *Physical Review B - Condensed Matter and Materials Physics*. 2007;75(19). doi:10.1103/PHYSREVB.75.195214

42. Singh T, Marom DM. Optical Communications. *Reference Module in Materials Science and Materials Engineering*. Published online 2017. doi:10.1016/B978-0-12-803581-8.00559-2
43. Ishigure T, Immonen M. Design and fabrication of multimode polymer waveguides for optical interconnects. *Optical Interconnects for Data Centers*. Published online November 14, 2016:171-195. doi:10.1016/B978-0-08-100512-5.00007-3
44. Scheidemantel J, Ambrosch-Draxl C, Thonhauser T, Badding V, Sofo O. Transport coefficients from first-principles calculations. *Physical Review B - Condensed Matter and Materials Physics*. 2003;68(12). doi:10.1103/PHYSREVB.68.125210
45. Madsen GKH, Singh DJ. BoltzTraP. A code for calculating band-structure dependent quantities. *Computer Physics Communications*. 2006;175(1):67-71. doi: 10.1016/J.CPC.2006.03.007
46. Scheidemantel J, Ambrosch-Draxl C, Thonhauser T, Badding V, Sofo O. Transport coefficients from first-principles calculations. *Physical Review B*. 2003;68(12):125210. doi:10.1103/PhysRevB.68.125210
47. Mikajlo EA, Dorsett HE, Ford MJ. Trends in the band structures of the group-I and -II oxides. *Journal of Chemical Physics*. 2004;120(22):10799-10806. doi:10.1063/1.1738635
48. Bolorizadeh MA, Sashin VA, Kheifets AS, Ford MJ. Electronic band structure of calcium oxide. *Journal of Electron Spectroscopy and Related Phenomena*. 2004;141(1):27-38. doi:10.1016/J.ELSPEC.2004.04.004
49. Whited RC, Flaten CJ, Walker WC. Exciton thermoreflectance of MgO and CaO. *Solid State Communications*. 1973;13(11):1903-1905. doi:10.1016/0038-1098(73)90754-0
50. Wu K, Liu T, Sun R, Song J, Shi C. First-principles calculations of oxygen vacancy in CaO crystal. *The European Physical Journal D 2020 74:10*. 2020;74(10):1-6. doi:10.1140/EPJD/E2020-10299-8
51. Chang ZP, Graham EK. Elastic properties of oxides in the NaCl-structure. *Journal of Physics and Chemistry of Solids*. 1977;38(12):1355-1362. doi:10.1016/0022-3697(77)90007-5

52. Suresh P, Balamurugan S, Balamurugan D. Electronic and optical studies of CaO with oxygen defects: A DFT approach. *Scholars Research Library Der Pharma Chemica*. 2014;6(4):292-297. http://derpharmachemica.com/archive.html
53. Mammone JF, Mao HK, Bell PM. Equations of state of CaO under static pressure conditions. *Geophysical Research Letters*. 1981;8(2):140-142. doi:10.1029/GL008I002P00140
54. Hoat DM, Naseri M, Rivas-Silva JF, Cocoletzi GH. Electronic, optical and thermoelectric properties of CaO mono- and bi-layers: Theoretical comparative investigation. *Optik (Stuttg)*. 2020;218:165115. doi:10.1016/J.IJLEO.2020.165115
55. Blinder SM. Density functional theory. *Introduction to Quantum Mechanics*. Published online 2021:235-244. doi:10.1016/B978-0-12-822310-9.00022-7
56. Hohenberg P, Kohn W. Inhomogeneous electron gas. *Physical Review*. 1964;136(3B): B864. doi:10.1103/PHYSREV. 136.B864/FIGURE/1/THUMB
57. Kohn W, Sham LJ. Self-consistent equations including exchange and correlation effects. *Physical Review*. 1965;140(4A): A1133. doi:10.1103/PHYSREV.140. A1133/FIGURE/1/THUMB
58. Vosko SH, Wilk L, Nusair M. Accurate spin-dependent electron liquid correlation energies for local spin density calculations: a critical analysis. *Canadian Journal of Physics*. 1980;58(8):1200-1211. doi:10.1139/P80-159
59. Ortenzi L, Mazin II, Blaha P, Boeri L. Accounting for spin fluctuations beyond local spin density approximation in the density functional theory. *Physical Review B - Condensed Matter and Materials Physics*. 2012;86(6). doi:10.1103/PHYSREVB.86.064437
60. Painter GS. Improved correlation corrections to the local-spin-density approximation. *Physical Review B*. 1981;24(8):4264-4270. doi:10.1103/PHYSREVB.24.4264
61. Svane A. Electronic structure of cerium in the self-interaction-corrected local-spin-density approximation. *Physical Review B - Condensed Matter and Materials Physics*. 1996;53(8):4275-4286. doi:10.1103/PHYSREVB.53.4275
62. Negele JW. Structure of finite nuclei in the local-density approximation. *Physical Review C*. 1970;1(4):1260-1321. doi:10.1103/PHYSREVC.1.1260

63. Yabana K, Bertsch G. Time-dependent local-density approximation in real time. *Physical Review B - Condensed Matter and Materials Physics*. 1996;54(7):4484-4487. doi:10.1103/PHYSREVB.54.4484
64. Zhang Y, Yang W. Comment on "generalized gradient approximation made simple." *Physical Review Letters*. 1998;80(4):890. doi:10.1103/PHYSREVLETT.80.890
65. Wu Z, Cohen RE. More accurate generalized gradient approximation for solids. *Physical Review B - Condensed Matter and Materials Physics*. 2006;73(23). doi:10.1103/PHYSREVB.73.235116
66. Perdew JP, Burke K, Ernzerhof M. Generalized gradient approximation made simple. *Physical Review Letters*. 1996;77(18):3865-3868. doi:10.1103/PHYSREVLETT.77.3865
67. Koller D, Tran F, B PBPR, 2011 undefined. Merits and limits of the modified Becke-Johnson exchange potential. *APS*. 2011;83(19):195134. doi:10.1103/PhysRevB.83.195134
68. Jiang H. Band gaps from the Tran-Blaha modified Becke-Johnson approach: A systematic investigation. *Journal of Chemical Physics*. 2013;138(13). doi:10.1063/1.4798706
69. Camargo-Martínez JA, Baquero R. Performance of the modified Becke-Johnson potential for semiconductors. *Physical Review B - Condensed Matter and Materials Physics*. 2012;86(19). doi:10.1103/PHYSREVB.86.195106
70. Koller D, Tran F, B PBPR, 2012 undefined. Improving the modified Becke-Johnson exchange potential. *APS*. 2012;85(15):155109. doi:10.1103/PhysRevB.85.155109
71. Blaha Karlheinz Schwarz Georg H Madsen Dieter Kvasnicka Joachim Luitz Robert Laskowski Fabien Tran Laurence D Marks PK, Blaha P, Schwarz K, et al. wien2k. *wien2k.at*.
72. Singh DJ. Adequacy of the local-spin-density approximation for Gd. *Physical Review B*. 1991;44(14):7451-7454. doi:10.1103/PHYSREVB.44.7451
73. Schwarz K, Science PBCM, 2003 undefined. Solid state calculations using WIEN2k. *Elsevier*. https://www.sciencedirect.com/science/article/pii/S0927025603001125
74. Schwarz K, Blaha P, Physics STM, 2010 undefined. Electronic structure of solids with WIEN2k. *Taylor & Francis*. 2010;108(21-23):3147-3166. doi:10.1080/00268976.2010.506451

75. Blaha P, Schwarz K, Tran F, Laskowski R, Madsen GKH, Marks LD. WIEN2k: An APW+lo program for calculating the properties of solids. *Journal of Chemical Physics*. 2020;152(7). doi:10.1063/1.5143061